Measurement report: Temporal variability of vertical profiles of CO_2 and CH_4 over urban environment

Mirosław Zimnoch[1,*], Michał Gałkowski[3,1,*], Piotr Sekula[2,1,*], Łukasz Chmura[1,2], Jakub Bartyzel[1], Alina Jasek-Kamińska[1,2], Alicja Skiba[1], Jarosław Nęcki[1], Paweł Jagoda[1], Michał Kud[1], and Przemysław Wachniew[1]

[1]AGH University of Krakow, Faculty of Physics and Applied Computer Science, Krakow, Poland
[2]Institute of Meteorology and Water Management — National Research Institute, Warsaw, Poland
[3]Max Planck Institute for Biogeochemistry, Department of Biogeochemical Signals, Jena, Germany
[*]These authors contributed equally to this work.

Correspondence: Miroslaw Zimnoch (zimnoch@agh.edu.pl)

Abstract. ~~Understanding the boundary layer dynamics over urban areas is important to improve estimates of the emissions of~~ Improving estimates of city-emissions requires a better understanding of the dynamics of pollutant transport in the urban boundary layer. This is particularly important for greenhouse gases (~~GHG), and predict their atmospheric mole fractions in these areas. Here~~ GHGs), given the role of urban areas in emission mitigation efforts. Given the inhomogeneity of emission sources and the complexities of atmospheric exchange and transport in urban environments, multiple and varied data streams are required to improve our direct understanding of urban atmospheric transport, as well as to provide inputs for modern inversion frameworks that can accurately estimate city-scale emissions. In this context, observations of the vertical distribution of GHGs are highly valuable. In this study, we present the results of ~~the annual vertical profiling measurement campaign~~ eleven measurement campaigns for vertical profiling performed in Krakow~~(Southern Poland). The campaign consisted of 11 monthly-based diurnal measurements~~ , southern Poland, over one calendar year (2022). These measurements aimed to provide high-resolution data on the vertical distributions of CO_2 and CH_4 ~~molar fraction vertical profiles supplemented by meteorological parameters focused on the investigation of the dynamics of nocturnal boundary layer vertical structure~~ mole fractions, alongside meteorological variables, within the urban ~~boundary layer. The profile data were collected using two~~ atmospheric boundary layer of Krakow, a mid-latitude humid continental city with a population of over one million. The data reported here form a basic dataset intended for establishing a city-scale inversion system. Additionally, the measurements presented here are valuable as high-resolution vertical profiles of GHGs within city limits and up to 280 metres above ground are difficult to obtain. The data were obtained using a Picarro G2311-f cavity ring-down spectrometer, which was deployed on two different platforms: (i) a tethered ~~touristic~~ tourist balloon operating commercially in the city centre, flying up to 280 ~~m~~ metres above ground level (a.g.l.), and (ii) ~~a drone system operating~~ an unmanned aerial vehicle (UAV) operating at altitudes up to 100 ~~m~~ metres a.g.l. ~~, with the selection of the platformbased on operational availability and meteorological conditions. and molar fractions were measured using Picarro G2311-f (Picarro Inc. , Santa Clara, California, USA) cavity ring-down spectrometer, while the meteorological conditions along the profile were measured using a set of~~ For the balloon deployment, the instrument was operated aboard the platform. In the case of the UAV, the analyser was connected through a 200-metre

tube. To our knowledge, this is the first time that such a method has been used for GHG vertical profiling. Additionally, meteorological conditions (temperature, relative humidity, pressure and wind) were measured using calibrated, low-cost sensors ~~dedicated for application on-board of~~ designed for use on UAV platforms. The ~~obtained results allowed~~ same set of sensors was used for both the balloon and the UAV. The results obtained in this study enabled us to analyse ~~in-depth the formation, development and disappearance~~ the characteristics of the urban boundary layer in depth, including its formation and development under various meteorological conditions throughout the year, with frequent observations of the nocturnal ~~boundary layer. In selected profiles, a~~ stable boundary layer possible thanks to the platforms' altitude range. Profiles were also observed in which CO_2 and CH_4 plumes~~located over the inversion layer (150-250 AGL) were detected during the nighttime~~, located above the stable boundary layer identified during the night-time and morning hours~~.~~, were detected. These are likely linked to emissions from strong localised sources outside the city. Overall, the presented data form a valuable scientific record that can be used for studying the behaviour of the boundary layer over urban areas (urban boundary layer, UBL), filling an important observation gap in the lowermost section of the troposphere over urban areas.

1 Introduction

Stabilising the global temperature rise in the XXI century ~~well~~ below 2 °C ~~, and toward 1.5 C,~~ requires comprehensive mitigation efforts targeting emissions of all greenhouse gases (~~GHG~~GHGs), including both CO_2 and non-CO_2 ~~GHG emissions (Ou et al., 2021). During 2022~~GHGs (Ou et al., 2021; IPCC, 2023). Despite several global policies already implemented (most notably the , the mole fractions of ~~three~~ the main atmospheric greenhouse gases emitted ~~by human activity (, and nitrous oxide),~~ through human activity continued their historically high ~~rates of growth in the atmosphere~~growth rates. The global ~~surface~~ average CO_2 dry air mole fraction rose by 2.13 ppm (1 ppm = 1 $\mu mol\,mol^{-1}$), reaching 417.06 ~~ppm~~ ppm in 2022 (NOAA, 2024)~~.~~ ~~The mole fraction of atmospheric~~ , and is now over 50 % higher than the pre-industrial level of approximately 280 ~~ppm~~ppm. Background levels of atmospheric methane in 2022 have also increased to an average of 1911.9 ~~ppb. Its annual increase was equal to~~ ppb, with an annual increase of 14.0 $ppb\,yr^{-1}$, the fourth largest annual increase recorded since NOAA's systematic measurements began in ~~1983, and followed record growth in 2020 and 2021.~~

~~The availability of dense GHG observation networks allows scientists to analyse both long-term trends and anomalies in carbon balance observed during the last decades. Knowledge of vertical GHG distribution is crucial for the evaluation of atmospheric models and , when profiles span full troposphere and lower stratosphere also in the calibration and validation of satellite-borne measurements. The low-level GHG profiles contribute indirectly to satellite data validation as well, through improving quality of the atmospheric models. All this components are necessary to improve the ability of atmospheric inversions to resolve emissions at regional and global scale (Keppel-Aleks et al., 2011).~~

~~On regional scales, the spatial and temporal distributions of and in the atmosphere are highly dependent on mesoscale weather systems (Zhang et al., 2022) and the distribution of their large-scale sources and sinks. On sub-regional and local scales, the crucial meteorological variables that determine the GHG variability, like wind speed, wind direction, and the planetary boundary layer (PBL) dynamics are superimposed on highly variable (both in space and time) distribution of sources~~

and sinks of GHGs (van der Woude et al., 2023). The variabilityin GHGs fluxes to the atmosphere is closely linked to the land-use and land-cover. In urban areas these are highly heterogeneous, and in addition to abundance of human activities responsible for GHGs release, the spatial and temporal distribution of their sources and sinks becomes extremely complex where urban environments are considered. On the other hand, GHG observations are still sparse in urban areas and the availability of high quality datasets is limited. Through atmospheric transport models, net GHG flux to the atmosphere can be transposed to its mole fraction observed in the local atmosphere. Most of the time, the local mole fractions are the result of the complex interplay between the sources, sinks, and the structure of atmospheric flows in the PBL. The atmospheric transport occurs not only in horizontal but also vertical directions, and the variability of the turbulence plays a critical role in shaping the vertical distribution of GHGs on diurnal scales (Li et al., 2014). It should also be noted that depending on local circumstances, GHGs mole fraction can also be affected by diverse topography (Giovannini et al., 2020), as interactions of the atmospheric dynamics with the orography can significantly influence the transport 1983. Growth rates of both primary GHGs remain high since over a decade, increasing concern over the realism of planned mitigation measures. A recent report from United Nations Environment Programme Programme (2025) estimated that the current global warming projections forsee a total global warming projection of between 2.3 °C and 2.5 °C by year 2100–assuming that all declared Nationally Determined Contributions are fully implemented. If only the policies already in place (as of the tracers on local or even regional scales. All these factors contribute to increased uncertainty of local dynamics of GHGs, and since the cities are their major sources, to the regional and in consequence the global inventory as well. In this perspective, providing observational data on the urban GHGs becomes crucial to improvement of emissions assessments2025), are considered the projected global average temperature is 2.8 °C, underlining the urgency of further mitigation efforts.

Research on the vertical structure of GHGs has been carried out in the past using multiple methods: stationary point measurements in the profile using the available tall-tower infrastructure (Richardson et al., 2017), tethered balloons (Li et al., 2014) , aeroplanes (Fiehn et al., 2020; Gałkowski et al., 2021), unmanned aerial vehicles (UAVs) using different sampling strategies like dedicated compact sensors (Kunz et al., 2018), discrete sampling (Lampert et al., 2020), or aircore systems (**?**) determining the measurements precision and temporal/vertical resolution, or with the use of either ground-based (Dietrich et al., 2021; TCCON, 2023) or spaceborne remote sensing (e.g. TROPOMI, GOSAT, Veefkind et al., 2012; NIES, 2023). The most precise and accurate sources of information on GHG vertical profiles are provided by air samples collected at different altitudes by using aircraft measurement systems (planes, balloons or UAVs) , as they can be relatively easily linked directly to WMO scales. They are also, however, usually sparse in space and time due to technical and logistic limitations, including lifting capacity, flight time and maximum reachable altitude. Besides that , they cannot operate during unfavourable weather conditions.

Urban areas, which constitute which constitute 2 % of the land surface, are responsible for around 70 % of anthropogenic fossil-fuel CO_2 emissions. Transport and buildings are among the largest contributors (Duren and Miller, 2012). A complex topography and land cover within urban areas strongly influence the boundary layer dynamics, being one of emissions (IEA, 2008; Seto et al , which makes them particularly interesting in the context of emission mitigation. However, due to the cultural, political and administrative differences, combined with extreme administrative, technical and financial complexity of implementation of city-wide policies targeting GHG emissions, the development of mitigation strategies for cities has been fragmented and

focused on largest, and usually wealthiest, agglomerations. One of the largest challenges in developing such policies results from the high spatial and temporal heterogeneity of urban GHG emissions. Dispersed sources with variable diurnal or seasonal variability, like road transport and individual heating, often contribute to the overall emission budget (Duren and Miller, 2012) , making the accurate quantification of emissions through bottom-up approaches challenging. In response, various top-down techniques for city emission monitoring have been developed. Direct estimations of city emissions using observations have been performed using in situ ground-based atmospheric observations (Lowry et al., 2001), airborne measurements using mass-balance technique (Mays et al., 2009; Turnbull et al., 2011; Cambaliza et al., 2014; Heimburger et al., 2017; Ashworth et al., 2020; Klausner et al., , and more recently using remote sensing total column observations, either from ground based instruments (Dietrich et al., 2021; Park et al., or from spaceborne sensors (e.g. de Foy et al., 2023). Each of these however has important limitations when it comes to monitoring of urban emissions, like biases from not including lack of representation of the full atmosphere (surface based), high measurement costs (airborne), low sensibility for weaker sources (remote sensing). More importantly, each direct emission estimation method heavily relies on assumptions regarding atmospheric flows in urban areas, for which additional observations datasets are valuable for more accurate wind fields, or for validation.

To overcome challenges in direct emission estimations, modelling frameworks based on Bayesian inversions have gained prominence, as they allow to represent complex atmospheric conditions, and to utilize limited observations to the ~~main physical drivers of dispersion processes in near-ground atmosphere. Especially the night-time vertical structure of the Urban Boundary Layer (UBL) , as well as the transition phase~~ maximum effect in a strict methodological framework. Inversion systems have been first developed for global Enting et al. (1995); Rödenbeck et al. (2003) and regional scales (e.g. Gerbig et al., 2003; Bergamaschi et al , but as the resolution of the models and their overall accuracy improved, city-scale inversions became feasible. One of the earliest attempts for application at the city-scale was reported by Lauvaux et al. (2013), and was followed by a series of studies in other cities (e.g. Lauvaux et al., 2016; Nalini et al., 2022; Chen et al., 2022; Ponomarev et al., 2026). Nowadays, inversion modelling is considered to be one of the recommended techniques in the World Meteorological Organisaton's report on Urban Emission Observation and Monitoring Good Research Practice Guidelines WMO (2025). In those modelling systems, one of the primary challenges is the existence of the transport model error, difficult to estimate and in most cases non-random. As accuracy of inferred emissions critically depends on the transport model's ability to correctly simulate the pollutant's dispersion, selection of appropriate model and fine-tuning of its setting are necessary steps for realistic emission estimates results. Despite gradual development of the models at the city scales, often spurred by activities within larger multi-partner projects like INFLUX (Lauvaux et al., 2016) or ICOS-Cities (ICOS-Cities, 2026), no standard solutions exist for high-resolution urban settings, and additional observations over various urban landscapes are necessary for setting up a modelling system for any new city.

High-resolution information in the Vertical profiles inside the cities is one of the most valuable data streams for modelling-based studies, as it provides information about processes, and at scales, most relevant to the transport model errors. Direct profile observations of meteorological data can be used to evaluate if the model setup and determine the accuracy of variables critical to pollutant dispersion (temperature, wind speeds and direction, and atmospheric boundary layer height over the city, denoted as UBL). Measurements of the lowest part of the troposphere are especially important. While meteorology within the city

is driven by mesoscale weather systems (Zhang et al., 2022), special phenomena occur (city canyons, urban heat island) that modify the atmospheric characteristics and GHG transport. Highly heterogeneous urban landscape drive the atmosphere in the city, and any modelling system need to realistically represent them. Simultaneously, emissions of GHGs occur on the same characteristic spatial scales, as many emissions are also tightly linked to land-cover (e.g. transport for CO_2, waste / sewage for CH_4) (Li et al., 2014; Giovannini et al., 2020; van der Woude et al., 2023). This means that for city applications models should be ideally used with ability resolve transport at resolutions of 100 m or below, in the lower range so-called "grey zone", in which model turbulence is partially resolved (Honnert et al., 2020). In practice, it has been shown that city-scale simulations of the GHGs can be run at coarser (1 km) resolutions using urban parameterisations of boundary layer processes developed for regional applications, provided that the transport error is carefully assessed (e.g. Lopez-Coto et al., 2020b, a; Peng et al., 2023) . While inverse frameworks using surface-data only, heavily supported by ceilometers and lidars for detection of the mixed layer have been employed (Lopez-Coto et al., 2020a), data from the atmospheric column can be of high benefit as sources located in the vicinity of measurement points might not yet be fully mixed across the UBL, potentially leading to biased estimations. Measurements in the lowest part of the troposphere also open the possibility of utilization of the nighttime data, discarded in most inverse modelling applications. Accurate representation of the vertical structure within the stable boundary layer (SBL) together with transition between stable and convective BL ~~, is crucial for a proper estimation of urban emissions based on a top-down approach using the high-resolution numerical models and ground-based atmospheric observations of GHG (Wei et al., 2020; Bezyk et al., 2023). One of the essential elements in such models is a proper parameterisation of the urban boundary layer(Lopez-Coto et al., 2020a; Peng et al., 2023). Validation of parameterisation schemes requires observational data containing both meteorological parameters and GHG mole factions in vertical profiles over the urban area. Obtaining such data anywhere~~ (CBL) (Lopez-Coto et al., 2020a). Ability to simultaneously measure vertical variability of meterorological variables and GHG profiles could then serve a double purpose - by helping to correctly fine-tune the modelling framework, as well as to provide data used for the inversion.

Research on the vertical structure of GHGs in urban areas can be attempted using in situ tall-tower infrastructure (Lowry et al., 2001; Rich , aeroplanes (Fiehn et al., 2020; Gałkowski et al., 2021), unmanned aerial vehicles (UAVs Kunz et al., 2018) or tethered balloons (Li et al., 2014). Airborne platforms are typically the best choice for this purpose, as only they allow measurements throughout the boundary layer. Atmospheric mole fractions of GHGs on airborne platforms can be done either by in situ sensors (e.g. Kunz et al., 2018; , through discrete sampling (Lampert et al., 2020), using aircore systems (Andersen et al., 2018). Remote sensing instrumentation can also be used for that purpose, but works published so far have mostly targeted point sources rather than cities (e.g. Krings et al., 2018; W . Especially over the densest parts of the cities, obtaining such data poses an organisational and logistical challenge, as measurements of vertical profiles require airborne platforms equipped with heavy instrumentation to achieve the necessary precision and accuracy. In ~~urban areas, the gathering of these data is even more constrained due to legal limitations; therefore~~addition, many cities limit the possibility to fly low over their central areas due to safety and security considerations. Consequently, the amount of ~~experiments targeting urban campaigns is relatively limited (e.g. Turnbull et al., 2011; Crawford et al., 2016; Park et al., 2017; Ashworth . Most studies targeting GHG fluxes that include sampling of the atmosphere throughout the vertical extent of the PBL~~ urban vertical profile data is still relatively limited, and most studies utilizing airborne sampling throughout the BL either limit

measurements to the areas ~~upwind or downwind~~ outside of the urban zones~~(Fiehn et al., 2020), or rely heavily on surface observations of GHGs supplemented by ceilometers and lidars for detection of the mixed layer (Lopez-Coto et al., 2020a).~~ , especially if mass-balance technique is attempted (Turnbull et al., 2011; Fiehn et al., 2020)

In this work, we report measurements of vertical distributions of ~~the basic meteorological parameters~~ basic meteorological variables (temperature, humidity, wind) and selected GHGs (CO_2, CH_4) within the urban boundary layer of ~~a city of ca.~~ Krakow, city of approximately 1 million ~~citizens, together with the description of their diurnal and seasonal variability. Over the course of the selected campaigns, distributions reaching elevations~~ inhabitants, collected over 11 single-day measurment campaigns throughout 2022. We have used two dedicated airborne platforms: i) a tethered touristic balloon operating in the strict city center as the primary platform, allowing for in situ measurements of up to 280 m ~~AGL and~~ a.g.l., and a UAV platform flying to the altitude of 100 m ~~AGL were observed using the balloon and UAV, respectively. The review of recent literature showed very limited avaiability of datasets containing UBL vertical profiles covering both, meteorological and GHG measurements covering diurnal as well as seasonal perspective. Most of published data are focused more on a long-term monitoring using stationary fixed elevation sampling points (Xueref-Remy et al., 2018; Hoheisel et al., 2023) or vertical profiles focused mainly on a short-term campaign-based measurements (Zhou et al., 2025; Bolek et al., 2024)~~ a.g.l. Both platforms used the same instrumental setup, including a precise weather station and a wavelenght-scanning cavity ring-down spectrometer (CRDS) Picarro G2311-f, either carried onboard (balloon) or connected to the airborne platform by a long tube (UAV). All reported measurements are directly linked to the appropriate WMO reference scales through calibration against standard reference gas mixtures. To the best of our knowledge, this is the first work reporting measurements by UAV connected to a high-precision instrument through a long tube for precise vertical profile measurements. Although Andersen et al. (2018) already showed an example of how this can be achieved when Aircore system is employed with UAV, with additional advantage of allowing for free flight path, unconstrained by the tube presence. However, their system has higher of spatial smoothing (due to mixing within the Aircore tubing) and is more complex in design, manufacture and data analysis. In studies in which dedicated on-board sensors were employed, lower measurement accuracy is usually achieved and more effort is needed to assure the link to the WMO reference scales (e.g. Zhou et al., 2025; Bolek et al., 2024).

We analyse the measurement data to discuss diurnal and seasonal variability of the GHGs in the lower troposphere over Krakow, with particular emphasis of boundary layer dynamics. We also present selected case studies for which a typical vertical structures were observed, likely linked to point source activity in the upwind areas. The presented measurements form the primary observational dataset for setup and validation of the inversion modelling framework for Krakow set up as part of the CoCO2 (Prototype System for a Copernicus CO_2 service) project ECMWF (2026).

2 Methods

2.1 Study area

Krakow is the second largest city in Poland, located in the Lesser Poland region, with an area of 326.8 km^2 and the number of inhabitants reaching over 800,000 according to official statistics (USK, 2023). The Krakow agglomeration consists of the city

itself and the highly populated towns and villages which surround it ~~, together with which the total number of people living in the area is estimated to exceed 1~~ forming a metropolitan areas with a total population reaches almost 1.4 million. The central part of the city is located in the Wisła (Vistula) River valley, at a mean altitude of about 200 ~~m~~ m above sea level (a.s.l.; Fig. 1). The valley is oriented along the west-east direction and surrounded by hilly terrain~~from the south (Western Carpathians region) and~~ : in the the south by Western Carpathians foothills, relatively flat upland areas from the north (Lesser Poland Uplands region) and scattered hilly ridges closing the valley from the west. The hilltops ~~bordering the city to the north and the south reach about~~ in the immediate vicinity of the city reach over 100 ~~m~~ m above the river valley floor, ~~similar to the hilltops in the western part of the valley. The surrounding hills form~~ and their elevation gradually increases to the south and to the north. Overall, surrounding topography forms a semi-concave landform open only to the east, partially sheltering the ~~lowest layers of the~~ lower atmosphere above the city from the ~~prevailing western winds~~overhead winds, usually westerly. A narrow opening immediately to the west (Krakow Gate) creates a passage through which the air can be channelled ~~if the wind conditionsare favourable (Figure 1). The~~ under favourable wind conditions. Multiple local scale processes ~~linked to the impact of relief include~~ are impacted by orography: it induces frequent air temperature inversions ~~,~~ in winter, promotes cold air pool formation ~~, air masses separation at the valley top (valley depth is equal c.a. 100 m), katabatic flows and much lower wind speed~~ with katabatic flows towards the river and reduces wind speeds in the valley floor ~~than at the hilltops (Sekuła et al., 2021b, a). These~~ as compared to areas over surrounding hills (Sekuła et al., 2021b, a). All these factors favour the accumulation of ~~trace gases emitted by local sources within the boundary layer over the city. Krakow represents~~ pollutants emitted within the city in the lower boundary layer.

Krakow's GHG emissions are representative of a typical urban environment, with ~~several~~ CO_2 driven by a mixture of anthropogenic and natural sources and sinks, ~~like low emission sources~~including households, industry, transport, water reservoirs and city biosphere~~, including citizens and their pets (Jasek-Kamińska et al., 2020).~~ . Here we understand biosphere as consisting of both natural and semi-natural flora and fauna, but also includes citizens and domesticated animals(Jasek-Kamińska et al., 2020) . Apart from distributed emissions, three major point sources are active within the city or in its immediate vicinity: Krakow Power Plant (PP; coal-powered, cogeneration plant), a steel mill located in an industrial compound, in the eastern side of the city (Steel Mill Krakow, ArcelorMittal Poland) and Skawina Power Plant (Skawina PP), located to the south-west 15 km of the Krakow centre (Fig. 1). A majority of CO_2 emissions from these sources are released into tall stacks. Krakow PP uses two main stacks, primary of 120 m and auxiliary, used in winter, of 260 m. Tall stack in Skawina is 120 m, and Steel Mill in Krakow emits primarily into two 200 m stacks.

Anthropogenic emissions of ~~methane are associated mainly~~ CH_4 are primarily associated with natural gas distribution ~~networks~~network, especially dense ~~and potentially leaking in urban centres and numerous landfills in the region (Zimnoch et al., 2019)~~ in urban centre, with heterogeneous and difficult to estimate leak rates. These are supplemented by emissions from wastewater network, limited industrial emissions (Steel Mill) and individual waste bins (Zimnoch et al., 2019; Menoud et al., 2021). Additionally, on the south-eastern city outskirts, a small municipal landfill (Barycz) is located, with no methane emissions reported in the Industrial Emission Database (Fig. 1 EEA, 2023).

~~Observations~~ Vertical profile sampling of GHG mole ~~fraction and meteorological parameters profiles were~~ fractions and meteorological variables was carried out using two ~~types of measurement platforms at~~ distinct measurement platforms operated at one of the two locations within the city: (i) a tethered touristic balloon operating commercially ~~close to~~ near the historical city centre (Balloon, 50.046°N 19.936°E), ca. 1800 ~~m~~ m south from the main market square in the Old Town ~~and~~ or (ii) ZFS-HEXA multi-rotor ~~drone platform operating next to the~~ UAV platform launched from the immediate vicinity of the building of the Faculty of Physics and Applied Computer Science~~(AGH site~~, within the campus of the AGH University of Krakow (AGH, 50.067°N 19.913°E~~), located within the campus of AGH University of Krakow, ca. 1800 m west from main market square in the old town (Figure 1). The balloon~~ , Fig. 1), 2.9 km to the north-west from the Balloon site. The Balloon site is located among recreational areas~~in the immediate vicinity~~ , 30 meters from the west bank of the Vistula River~~. The surrounding area is~~ , with the surrounding area made up of promenades ~~, green areas . Within a~~ and green areas to the north and the south, and a busy communication artery passing 130 meters to the west. Within the radius of one kilometer~~there are~~ , only buildings connected to the ~~minicipal heating network . From the west, the site is adjacent to a busy communication artery. The drone flights were performed within AGH University of Krakow campus. The surrounding area includes university~~ municipal heating network have been identified, i.e. those without individual combustion sources. The UAV measurements were carried out at AGH site due to lack of necessary infrastructure at the Balloon Site. Near AGH site, the surrounding area is more densely populated, mainly surrounded by university or private residential buildings connected to the ~~heating system as well as a park and a sports stadium . The neighbourhood is dominated by green areas to the south,~~ central heating system. A large sports stadium and a major city park are located immediately to the to the south and ~~multi-family housing and~~ south-east, respectively, and a busy road passes 100 m to the north. ~~In both locations surface emissions are dominated by biogenic activity and transport emissions. In case of , previous studies have identified city gas network leakages, as a main emission source. Due to complex structure and not well known technical condition, which is the subject of continous routine network operator activities, it is hard to point a specific locations as a potential methane emission sources. Auxiliary meteorological parameters were also measured on the roof of the faculty building. The direct distance between measurement sites was 2.9 . Co-located measurements were impossible due to legal restrictions constraining the possibility of UAV operations at the balloon location.~~ Overall, both sites are located well within the city centre and no significant differences in the characteristics of the boundary layer are expected.

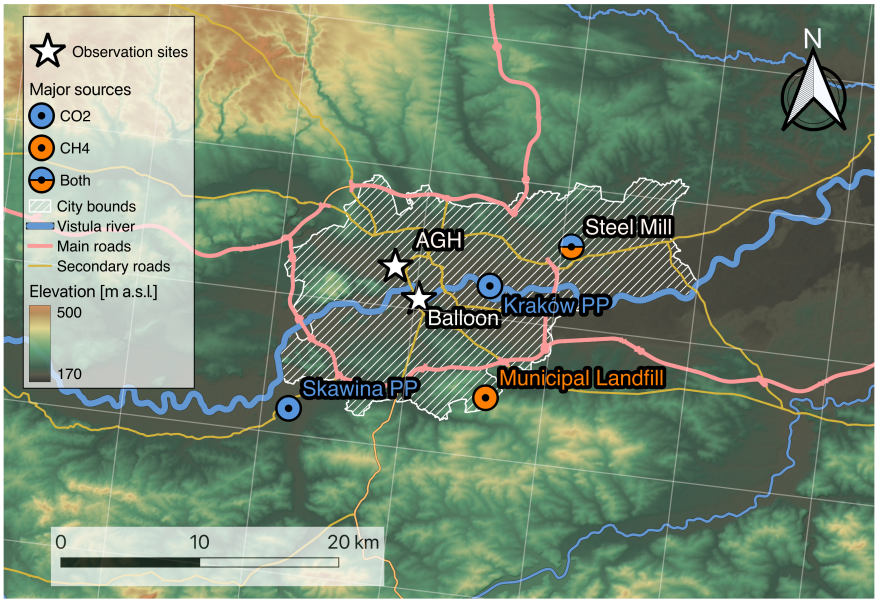

Figure 1. Study area with points of interest overlaid on the topography map. PP - power plants (coal powered cogeneration plants.)

2.2 Measurement techniques

2.3 ~~Measurements of vertical profiling of GHGs and meteorological parameters~~

2.2.1 Flight organisation and schedule

Vertical profiles of CO_2 and CH_4 presented ~~in the article~~ were measured with the use of two ~~aireraft~~ airborne platforms - a sightseeing tethered balloon (~~8~~ eight campaigns) and a UAV (~~3~~ three campaigns). The maximum flight altitude for the ~~drone~~ UAV was equal to 100 m ~~AGL which was determined~~ a.g.l., a maximum allowed by the aviation regulations~~for measurement location~~. In the case of the balloon, the maximum flight altitude varied over the campaigns between 100 and 280 m ~~AGL~~a.g.l., depending on the ~~vertical wind profile and the number of passengers. During working hours, the flight schedule depended on the~~ wind strength across the profile and, during the day, the number of passengers ~~willing to fly (on average~~ onboard. If passengers where present, flights were executed approximately every 15 minutes~~), while during the nighttime hours, flights were made~~ , otherwise they occurred at approximately hourly intervals. ~~Drone~~ UAV flights were performed in hourly intervals~~during all the campaigns~~. The timing of the measurement campaign was mostly determined by meteorological conditions~~. The~~ , with the decision to fly on a given day ~~was first made~~ based on the ~~current~~ availabe weather forecast (IMGW-PIB, 2023)~~analysed by the flight operator of a drone or sightseeing balloon~~. The factors ~~precluding flying include~~ preventing flying included the occurrence or forecast wind gusts above 8 $\mathrm{m\,s^{-1}}$ (~~for UAV wind speed~~ or greater than 10 $\mathrm{m\,s^{-1}}$ for UAV), the risk of storms or the incoming atmospheric front~~; balloon icing; too~~ , balloon icing, low air temperature (for balloon below -10°C)~~;~~ ,

Table 1. Campaigns details, ~~flight~~ flights were conducted with the use of two aircraft systems - sightseeing balloon and UAV - at two locations: for balloon (signed as BAL) - 50.046°N 19.936°E, 207 ~~m~~ m a.s.l.; for UAV - 50.067°N 19.913°E, 220 ~~m~~ m a.s.l.

No.	Date	Sunrise (UTC)	Sunset (UTC)	First flight (UTC)	Last flight (UTC)	Flights number	Platform type
1	10-11.03.2021	05:10	16:30	20:20	07:00	12	BAL
2	28-29.04.2021	05:20	17:50	19:00	08:00	15	BAL
3	01-02.06.2021	02:40	18:40	08:45	05:00	44	BAL
4	13-14.07.2021	02:40	18:50	17:40	06:20	28	BAL
5	07-08.09.2021	04:00	17:10	15:20	08:00	29	BAL
6	11-12.10.2021	04:50	16:00	17:00	07:00	13	UAV
7	25-26.10.2021	05:15	15:30	16:20	10:00	27	BAL
8	24-25.11.2021	06:05	14:50	13:20	12:00	34	BAL
9	22-23.12.2021	06:40	14:40	14:10	11:30	21	BAL
10	11-12.01.2022	06:40	15:00	14:00	05:00	16	UAV
11	31.01-01.02.2022	06:20	15:20	14:00	10:15	19	UAV

strong atmospheric precipitation or low visibility. ~~The measurements were performed mostly at night . The~~ Each measurement campaign (except June 2021) was performed between afternoon or early evening, and run through the whole night until finish in the morning, in order to capture a full cycle of UBL development. The longest campaign lasted from 08:45 UTC to 05:00 UTC the next day and included 44 flights, and the shortest from 20:20 UTC to 07:00 UTC next day, with a total of 12 flights. The balloon's flight vertical speed did not exceed 1 $\mathrm{m\,s^{-1}}$. The ~~flight~~ ascent time depended on the maximum altitude and ranged from 2–3 ~~min (for maximum height equal to~~ min (maximum height of 100 m ~~AGL~~a.g.l.) up to 6–~~10 min~~ 10 min (for maximum height ~~equal to~~ of 280 m ~~AGL~~a.g.l.). For the UAV flights, the vertical speed of the ~~drone~~ UAV also did not exceed 1 $\mathrm{m\,s^{-1}}$, ~~on average it was equal to~~ with the average of 0.5 $\mathrm{m\,s^{-1}}$. The ~~flight~~ ascent time for the UAV system varied from ~~5 to 10 min~~2 to 5 min. Table 1 contains detailed information about each measurement campaign, including the type of platform and number of performed flights. ~~Campaign~~

All times in the study are reported in Coordinated Universal Time (UTC). Kraków's timezone is Central European Time, which corresponds to UTC+1 (standard time, late October—late March) or UTC+2 for daylight saving time (late March—late October). Sunrise and sunset times were calculated using the algorithm provided in the Almanac for Computers (Nautical Almanac Office, 1 . More detailed campaign characteristics, including flight ~~take-off and histogram of maximum flight altitudes~~frequency and flight altitude distributions, are presented in Figure ~~S2~~ S1 in the Supplement.

2.2.2 Observation platforms

~~At the balloonplatform~~On the balloon, a set of meteorological sensors was fixed to the outer side of the ~~gondola while the~~ passanger gondola. The Picarro G2311-f analyser and battery power supply system was placed ~~in the balloon gondola. The~~ inside the gondola, with the air inlet was installed 3 m above the ~~balloon gondola~~gondola's deck, protruding towards the exterior by 30 cm, to avoid contamination with CO_2 exhaled by the passengers ~~. In the case of the~~ (Figure 2A). On the UAV system, a suite of meteorological sensors consisting of air temperature, relative humidity, atmospheric pressure, and wind speed was installed on top of the ~~drone~~UAV platform. In order to minimise the influence of turbulence generated by the propellers and provide proper ventilation of meteorological sensors and air inlet (GHG measurements), ~~they~~ these were located in the middle part of a UAV and elevated ca. 25 cm above the propeller height (similar to McKinney et al., 2019; Hedworth et al., 2022). ~~Wind~~ The air inlet at the top of the UAV was connected through a 200 m long 1/8" OD tube to the same Picarro analyser installed in the Gas Laboratory inside the Faculty building. It should be noted that wind direction measurements were not considered in the current study due to the horizontal oscillations of the balloon ~~and drone~~ during the flight~~and the~~ . During UAV flights, the data were also rendered unusable due to the strong interference of the electronic compass with the magnetic field generated around the power cables of the ~~drone motors~~ UAV motors (Figure 2B).

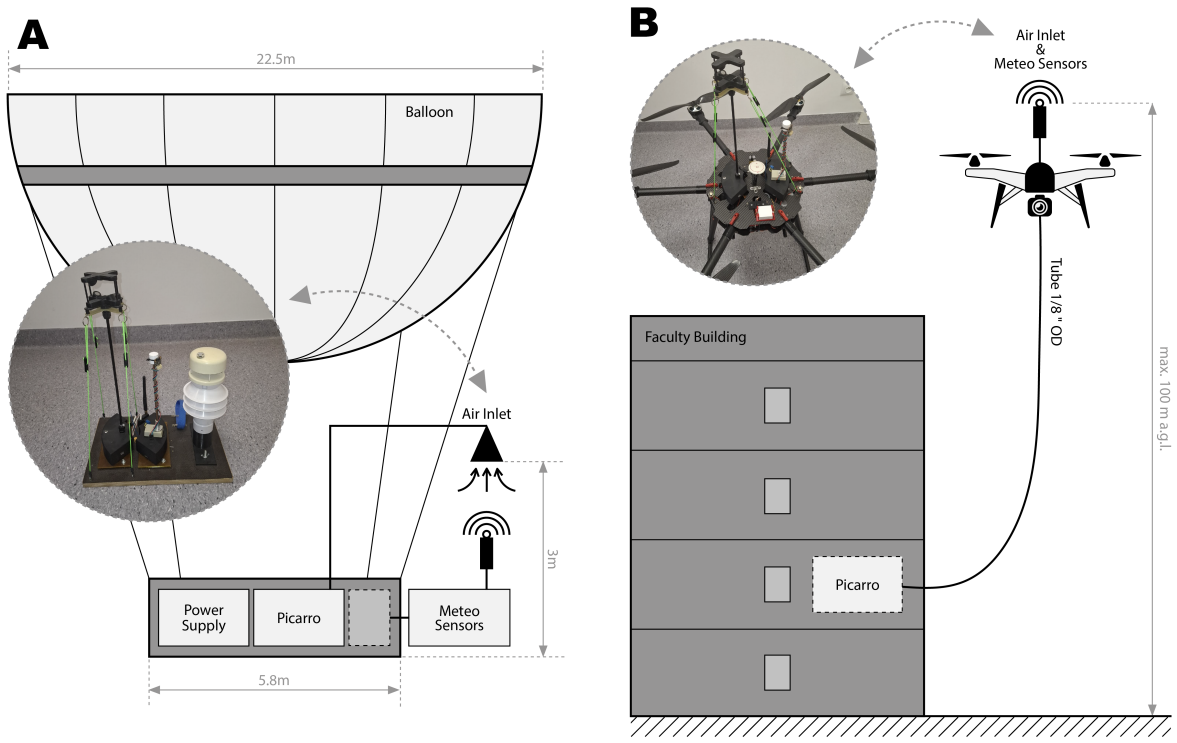

Figure 2. Measurement setup for platforms used in the study. A - balloon. B - UAV system.

To provide detailed information on the location of the measurement, the system was equipped with a GPS receiver ~~and meteorological sensors providing e.g. the altitude estimated with combined GPS and barometer signals~~(NEO-7 GNSS module, u-blox AG, Thalwil, Switzerland). A detailed analysis has shown that the altitude calculated from the barometric formula (Equation 1) is more precise than GPS measurements (~~Equation 1).~~ Figure S2), therefore the position was estimated using a combination of GPS and barometer signals for horizontal and vertical location, respectively.

$$h = \left[\left(\frac{P}{P_0} \right)^{1/5.257} - 1 \right] \times \frac{T}{0.0065} \quad (1)$$

Where: h - altitude in m ~~AGL~~a.g.l.; P_0 - atmospheric pressure at the surface level in hPa; P - atmospheric pressure at the current position in hPa; T - air temperature at the current position in K.

~~Based on the analysis of the obtained data and the literature review, it was assumed that only the~~ In this study, only measurements collected during the ascent were ~~representative of atmospheric conditions in the vertical profile. In the case of balloon campaigns, during the descending~~ considered. During the flight, the balloon often ~~began to rotate~~rotated and oscillated horizontally during the descent, which had a significant impact on the measurement of meteorological ~~parameters (visible on~~ variables (especially wind measurements) and GHGs mole fractions under specific conditions. In the case of ~~the~~ ascending flight, ~~the rotation of the balloon was much~~ these movements were much gentler and less frequent. Furthermore, ~~since~~ due to the air inlet ~~was located~~ location above the balloon gondola, ~~during the descent~~ it was possible that the measured air might ~~be~~ become contaminated with the passengers~~breathing~~' exhaled air during the descent. For UAV-based measurements, ~~recent studies~~ a recent study by Hedworth et al. (2022) indicated that vertical measurements of gaseous pollutants during ~~the ascent are characterised~~ ascent are characterized by the lowest relative error (on the order of a few %)~~. During the descentof the drone, depending on atmospheric stability conditions,~~, while during the descent, the relative error of measured mole fractions of gaseous pollutants may be even an order of magnitude higher~~(Hedworth et al., 2022)~~, depending on atmospheric stability conditions.

2.2.3 Measurements of CO_2 and CH_4 mole fractions

Measurements of carbon dioxide and methane mole fractions ~~presented here~~ were performed by CRDS Picarro G2311-f analyser ~~.~~ (Picarro, Inc., USA). For vertical profiling, the instrument operated in the ~~Flux (Low Flow) mode~~flux mode (low-flow mode), enabling measurements with a precision of 0.2 ~~ppm~~ ppm for CO_2 and 3 ~~ppb~~ ppb for CH_4 at a frequency of 10 ~~Hz~~Hz. Before and shortly after each measurement campaign ~~listed in Table1~~(Table 1), a calibration procedure was performed~~. It involved measuring mole fractions of two standard mixtures~~ , similar to the standard procedures employed within the ICOS (Integrated Carbon Observation System) atmospheric network (ICOS RI, 2020). The calibration procedures were as follows: for one hour, the GHG mole fractions in the two standard dry mixtures (calibrarion standards) of known composition ~~for one hour each. In the course of each campaign, a total of eight standard mixtures were used~~were measured by the CRDS instrument. Two mixtures were selected from the cylinders available in the lab, ranging from ~~374 to 521 ppm~~ 380 to 524 ppm for CO_2, and from ~~1880 to 2641 ppb~~ 1883 to 2289 ppb for CH_4. ~~The set of calibration~~ Calibration standards consisted of two primary

standards provided by the ~~Integrated Carbon Observation System (ICOS) calibration centre and six~~ ICOS Central Analytical Laboratories (D048624, D048638) and four working standards produced ~~in the greenhouse gas measurement laboratory at AGHUniversity of Krakow. For maintaining the WMO scale the laboratory is participating in a periodic intercomparison excercises~~in-house at AGH. All results presented here are reported in WMO GAW (Global Atmospheric Watch) scales, WMO X2019 for CO_2 and WMO X2004A for CH_4 after applying the linear calibration corrections based on calibration curves ($y = 1.001x + 2.7192$ for CO_2 and $y = 0.996x + 12.109$ for CH_4), obtained from collective calibration data obtained over all measurement campaigns. To avoid measurement contamination by human respired CO_2 during the balloon campaigns, a 10 m long 1/8" OD inlet tube was used allowing to place the air inlet ca. 3 m above the balloon gondola. In the case of ~~drone~~ UAV campaigns 200 m long, a ~~4~~ 1/8" OD inlet tube was used to connect the air inlet fixed to the UAV with the stationary analyser, located in the laboratory. The Picarro pump was sufficient for flushing the tube. Inlet tubing introduced a signal delay which was determined before each campaign through a ~~breath test~~ simple test performed by injecting CO_2-rich air respired by the operator and measuring the response time of the analyser (Figure ~~S1). The final reported values were obtained by correcting the raw data using the calibration lines ($y = 1.001x + 2.7192$ for and $y = 0.996x + 12.109$ for)obtained during all available calibration proceduresS3 in the Supplement~~). In the case of both species, the correlation coefficient R^2 for calibration lines was equal to 1 within four significant digits. The maximum long-term drift of measured standards ~~molar~~ mole fractions was 0.2 ~~ppm~~ ppm for CO_2 and 1 ~~ppb~~ ppb for CH_4, respectively. We applied internal instrument water correction, which is sufficient in the typically observed ranges of water vapour mole fractions (from tenths to ca. 2.5%)(Reum et al., 2019).

2.2.4 Sensors for meteorological ~~parameters~~variables

The profiles of meteorological ~~parameters~~ variables presented in the article were measured using three measurement systems forming the basic set: the AirDust system (designed and constructed in-house at the Environmental Physics Group, AGH University of Krakow), the sonic anemometer TriSonica™ Mini Wind and Weather Sensor (Anemoment LLC, Longmont, CA, USA) and the Mini Weather Station (HY-WDC6SE, HONGYUV, China). The auxiliary stationary measurements are described in the next chapter. The AirDust system ~~and the acoustic wind sensor TriSonica™ were dedicated for measurement~~ was dedicated for measurements with the use of ~~unmanned aerial vehicle (Sekuła et al., 2021c) . To provide meteorological sensor redundancy during the balloon campaigns, the~~ both UAV (Sekuła et al., 2021c) and balloon platforms. The acoustic wind sensor TriSonica™ was used with the UAV, while HY-WDC6SE Mini Weather Station ~~(HY-WDC6SE) was used. Due to its size and weight as well as the difficulty in mounting it over UAV, it was not used in drone measurements. For balloon measurements, it was possible to use all three systems in parallel thanks to the substantially larger lifting capacity and available space than in the UAV-based system. Due to a number of technical complications, measurements of meteorological parameters in individual sampling campaignswere carried out by different sets of sensors. Detailed information on sensor specifications used in the study is summarised in Table 2. As the individual sensors varied in their sensitivities response times, we have selected the best-performing of the available data for our analysis. Table S1 compares individual meteorological parameters measured by sensors deployed in balloon and UAV-based campaigns. Information on which sensors were used in each campaign is listed in Table S2~~in balloon campaigns. All three systems had duplicated sensors to provide redundancy during the campaigns.

AirDust measurement system

The ultra-light measurement AirDust system was dedicated to meteorological measurements within the urban boundary layer. The system was based on the Arduino MKR ZERO microcontroller, responsible for communication between the sensors and for storage of the measurements on the memory card. The system was powered by a drone battery via a step-down converter reducing the input voltage from 22 V to 5 V at 2 A. Air temperature, relative humidity and atmospheric pressure In the majority of flights, the temperature, pressure and relative humidity were measured using a digital sensor (BME280, Bosch Sensortec GmbH, Reutlingen, Germany). To monitor temperature changes within the given vertical profile with a better spatial resolution, the systemwas also equipped with a thermocouple type T. Since the response time of the T-type thermocouple to temperature changes is shorter than for the BME280 sensor, by default, the measurement was taken from the thermocouple. For the corrections of thermocouple bias error and in the event of technical issues with the thermocouple, the BME280 sensor was used. The sampling frequency of the AirDust system was set to 1 Hz. Technical specification of the AirDust system is presented in Table 2.

TriSonica™ anemometer

The second measurement system used in the measurement campaigns was based on the acoustic anemometer TriSonica™. It was used to monitor horizontal wind components in the studied vertical profile. The system was equipped with an Arduino MKRZERO microcontroller for data storing and the NEO-7 GNSS module (u-blox AG, Thalwil, Switzerland) which allows monitoring of the horizontal and vertical position of the sensors. The TriSonica ™ sensor is equipped with a 3D sonic anemometer, temperature, pressure and humidity sensors, as well as a magnetometer and 3D accelerometer for correcting the wind speed and wind direction. The measurements of air temperature, pressure and humidity from the TriSonica sensor were not used in this study due to the fact their inertia was larger than those used in the AirDust system. To avoid measurement disturbances caused by turbulence generated by the drone's propellers during the UAV-based campaigns, the system was fixed on a small extension arm ca. 30 cm over the drone platform. The anemometer can measure wind speed and wind direction with different sampling frequencies, from 1 to 10 . It was found that measurements with a sampling frequency equal to 1 were characterised by the smallest number of incorrect measurements (glitches). Therefore, the frequency of the system was set to 1 . Analysis of the wind direction observations in the vertical profile revealed that reliable measurements were difficult to achieve. The idea of wind direction correction using an onboard magnetometer during the flight was tested (balloon and UAV-based campaigns). In the case of UAV-based campaigns magnetic field disturbance generated by the currents supplying the drone's motors generated too much noise making it impossible to use a magnetometer for a correction procedure. Finally, wind direction measurements in vertical profiles were excluded from further analysis due to their unreliability. The AirDust system, while the wind speed was measured by TriSonica Mini or HY-WDC6SE sensors. The other redundant sensors were used on per-need basis in case of the primary system failure (see Table S2). The technical specification of the TriSonica™ sensor was included basic set is summarised in Table 2(only wind speed measurements). , and the full sensors description, specifications and configurations are described in the Supplement.

Mini Weather Station

Table 2. Technical specifications of ~~three~~ basic set of meteorological systems.

~~Bosh BME280 (AirDust system)~~ Parameter	Operating ra
Bosh BME280 (AirDust system)	
Relative Humidity	0 ÷ 100 %
Air Pressure	300 ÷ 1100
~~Temperature -40 C ÷ 85°C ±1 C 0.01 C~~ Dimension/Weight	
Thermocouple type T (AirDust system)	
Temperature	-50 °C ÷ 15
TriSonica™ sonic anemometer - UAV campaigns	
~~Parameter Operating range Accuracy Resolution~~ Wind Speed	0 ÷ 50 m s⁻
Dimension/Weight	
Mini Weather Station (HY-WDC6SE) - balloon campaigns	
~~Parameter Operating range Accuracy Resolution~~ Wind Speed	0 ÷ 40 m s⁻
~~Relative Humidity 0 ÷ 100 % ±5 % 1 % Air Pressure 150 ÷ 1100 ±1 0.1 Temperature -40 C ÷ 80 C ±0.5 C 0.1 C~~ Dimension/Weight	

~~The Mini Weather Station was used to monitor horizontal wind speed, air temperature, relative humidity and atmospheric pressure in a vertical profile. It is worth mentioning that the inertia of air temperature and relative humidity sensors in the Mini Weather Station is larger than for the sensors used in the AirDust system. Due to this fact, the Mini Weather Station was used as a backup system for AirDust sensors. The Mini Weather Station provides also measurements of atmospheric precipitation and radiation components which were not used in this study. The sampling frequency of the HY-WDC6SE station was equal to 1 Hz. Technical specification of the Mini Weather Station for selected meteorological parameters is presented in Table 2.~~

~~Sensors calibration~~

Calibration of all meteorological sensors was performed through a comparison against the stationary meteorological station operating at the AGH site (see Sections 2.1 and 2.3). Air temperature, relative humidity, atmospheric pressure and wind at the level of 20 m ~~AGL~~a.g.l., were measured using a WXT520 weather station (Vaisala, Vantaa, Finland)~~weather station. Figure S3~~ . Figure S4 in the Supplement presents the comparison between tested sensors and reference instruments over three consecutive days (from 29 April to 2 May 2022) with one-hour resolution, together with linear regression equations for individually tested ~~parameters~~variables. The calibration equation and correlation coefficient R^2 obtained with the use of linear regression are presented in Table 3. For ~~calibration~~ all instruments except anometers, the formula $y = Ax + B$ was used in the calibration. For calibration of the anemometers, the intersection points of the regression lines were set to 0. Tests of the sensors showed the correct measurement for atmospheric calm ~~, where the~~ (wind speed was equal to 0 $m\,s^{-1}$~~. For the remaining instruments, the formula $y = Ax + B$ was used in the calibration.~~). Formulas of linear regression were ~~used to~~ applied to raw data to correct the systematic ~~error of~~ errors and make the measurements presented in this article consistent regardless of the specific sensor used at a given time.

Table 3. Meteorological sensors calibration details. All anemometers were calibrated using the $y = Ax$ formula, for all other instruments $y = Ax + B$ was used.

Sensor ID	Meteorological parameter	R^2	Equation
Meteo WDC6SE	Wind speed	0.95	$y = 0.95x$
	Air temperature	0.99	$y = 1.02x - 0.62$
	Atmospheric pressure	0.99	$y = 1.01x - 7.26$
	Relative humidity	0.99	$y = 1.06x - 3.07$
TriSonica	Wind speed	0.96	$y = 0.85x$
Thermocouple	Air temperature	0.99	$y = 1.02x - 0.89$
BOSH BME280	Air temperature	0.99	$y = 0.98x + 0.73$
BOSH BME281	Atmospheric pressure	0.99	$y = 1.04x - 34.50$
BOSH BME282	Relative humidity	0.99	$y = 0.96x - 1.60$

2.3 Auxiliary ~~stationary~~ in situ measurements

In addition to measurements conducted directly at the site of the measurement campaigns, continuous observations of meteorological ~~parameters~~ variables and CO_2 and CH_4 mole fractions were carried out on the university campus in the location of ~~drone~~ UAV flights providing data representing the urban boundary layer in the vicinity of the campaigns. Meteorological measurements were conducted using the Vaisala WXT520 weather station located on the roof of the Faculty of Physics and Applied Computer Science building (50.067°N 19.913°E~~) ca. ,~~ 20 m ~~AGL~~ a.g.l.). The station has been operating at this location since 2012 and provides long-term one-minute temporal resolution information about the ambient temperature, relative humidity, atmospheric pressure, wind speed, wind direction and precipitation ~~. The meteorological dataset is supplemented by the radiation dataset collected with an NR01 (Hukseflux Thermal Sensors B.V., Delft, The Netherlands)net radiometer installed at the same location ca. 40 AGL The radiometer consists of two sets of sensors for different wavelength ranges (a pyranometer and a pyrgeometer), one set facing up and another facing down, enabling measurement of all components of net radiation balance.~~ (see Supplement). In addition to meteorological measurements, observations of CO_2 and CH_4 ~~molar~~ mole fractions in the periods between profiling campaigns were also carried out continuously using the same Picarro analyser for profile measurements. The air inlet was placed ~~at the location of the net radiometer (~~ca. 40 m ~~AGL).~~ a.g.l.).

We have also used the CO_2 and CH_4 atmospheric dry air mole fractions observed from the KASLAB GHG observation station at Kasprowy Wierch (49°14'N, 19°59'E, 1989 m a.s.l.) as background for the urban measurements. It is located in the Tatra Mountains, approximately 120 km south from Krakow, and has been providing data since 1994.(Rózanski et al., 2016), and is a GAW regional station.

2.4 Estimation of urban boundary-layer height

In the subsequent analysis, for cases where clearly defined layering was identifiable, we calculated the height of the Urban Boundary Layer (UBLH) as the altitude at which measured mole fractions of the CO_2 (or CH_4) reach the value corresponding to half the difference between well-defined lowest and highest values, corresponding to either residual layer or boundary layer. We have discarded five percentile of data in both extremes to account for local-scale noise. While this method has certain limitations, it is easy to apply and, contrary to thermodynamic-based methods (e.g. using the potential temperature gradient or bulk Richard it allows to calculate the layer relevant to height of mixing, most relevant in target applications concerning transport and emissions of GHGs. The detailed algorithm of the calculation is as follows.

First, the profiles were visually filtered to exclude enhanced values in the lowest 5 meters (for CO_2 those could be caused by high enhancements directly at surface likely due to exhaled breaths of crew, tourists, passers-by etc.; for CH_4 no clear cause was identified). Second, the any enhancements above the UBL, related to long-range transport, have been excluded from the dataset as they would distort the residual layer values (see sections 3.3 and 3.4). Third, for each vertical profile, values below the 5^{th} and above the 95^{th} percentile were discarded. The remaining data formed a filtered profile dataset. In the fourth step, mole fractions of the 5^{th} and 95^{th} of the mole fraction value were marked as GHG_{min} and GHG_{max}, representing residual layer or the boundary layer values. Here, the percentiles were used rather than minima and maxima to avoid distortions due to small variabilities of mole fractions within UBL and residual layer. UBLH was determined as the height at which the mole fraction profile crossed the mean of GHG_{min} and GHG_{max}. If the above condition was met multiple times for a single vertical profile, the UBLH was designated as the average of all such heights. Finally, to ensure the accuracy of the obtained boundary layer height, the profiles were for a given campaign were inspected visually (together with the meteorological profiles), to exclude a limited number of events where the UBLH was identified as false positive (afternoon flights, convective boundary layer).

3 Results and Discussion

3.1 Overview

Stationary measurements of GHGs at AGH site (AGH University of Krakow, Faculty of Physics and Applied Computer Science, 50.067°N 19.913°E) during the period from March 2021 till April 2022 illustrates a seasonal (Figure 3~~a~~A and B) and day-to-day (Figure 3~~b~~C and D) variability of CO_2 and CH_4 respectively at the constant altitude of 40 m ~~AGL~~ a.g.l. in the location close to the city centre ~~.~~ (black symbols) compared to the regional background observed at the KASLAB high mountain station located ca. 100km south from Krakow in Tatra Mountains (blue symbols). The lowest monthly mole fraction of CO_2 and CH_4 was measured in May and the highest in October and are well correlated with the difference between levels observed in the UBL compared to the regional background. An annual amplitude calculated based on monthly mean values was equal to 25 ~~ppm~~ ppm and 120 ~~ppb~~ ppb for CO_2 and CH_4 respectively. The locations of minimum and maximum values are determined by two factors: (i) the seasonal variability of source/sink activity; and (ii) the intensity of mixing processes occurring in the UBL. A larger day-to-day change observed on the daily means recorded during the cold season is the result of the higher intensity of anthropogenic emission sources in this season and the significant influence of the synoptic situation on the daily mean values.

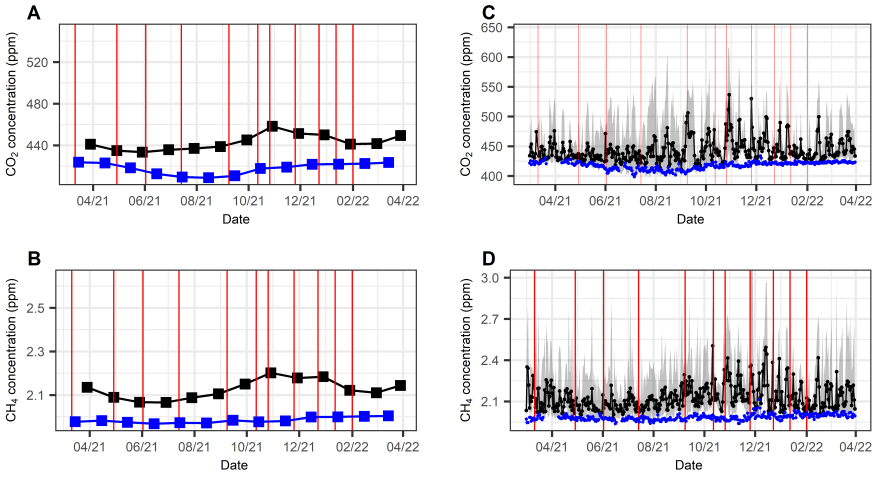

Figure 3. Monthly (~~A~~A-B) and daily (~~B~~C-D) ~~mean~~ means of CO_2 and CH_4 mole ~~fraction~~ fractions from AGH site (dark line) at 40 m ~~AGL~~ a.g.l. measured using a Picarro G-2311-f analyser and from KASLAB high-mountain station (blue line) for the period from March 2021 to April 2022. The grey shading in panels C–D indicates the diurnal variability at the AGH site, defined as the daily minimum and maximum mole fractions. The dates of vertical profile measurement campaigns are marked by vertical red lines.

Figure 4 presents the Box and Whisker Plot showing the data distribution of CO_2 and CH_4 mole fractions during each campaign representing the variability observed at three different altitude ranges (20-50m, 80-100m and 180-200m a.g.l. within the city and regional backgroud. It can be seen that the values observed in the highest layer of the urban atmosphere are close to the regional background value, but their variability is often slightly greater, which is the result of the proximity of emission sources compared to the mountain station. In turn, the highest values and the greatest variability are observed in the lowest layer. In case of CO_2, a greater scatter of data observed in the lowest layer exists in summer compared to the winter time, while in case of CH_4 the scatter seasonal variability is less pronounced. This suggests a methane emissions in the city are consisting of a relatively constant source (leakages in the city gas network) and partly by temperature-dependent processes (like municipal waste and sewage system). The intensity of CO_2 sources in turn varies throughout the year with changes in biosphere activity (respiration and assimilation processes).

Systematic measurements of CO_2 and CH_4 vertical profiles (Figure 5) allowed us to study their variability on different timescales in an urban environment of Krakow. Distinct seasonal and diurnal variability is observed when data is ~~grouped~~ filtered accordingly: by seasons (colours) and time of the day (panel columns). CO_2 mole fraction varied with altitude depending on time of day. During the day, turbulent mixing of air within the boundary layer averaged the mole fraction within the profile, and CO_2 emissions from anthropogenic and biogenic sources having it's own diurnal pattern in the area were compensated by the photosynthesis sink. During the night, diminishing of photosynthesis caused the increase of the net CO_2 flux from the surface, and as a result, together with stable boundary layer (SBL) formation, accumulation of CO_2 near the surface was observed. At the same time, CO_2 mole fraction within the higher part of the profile remained constant regardless

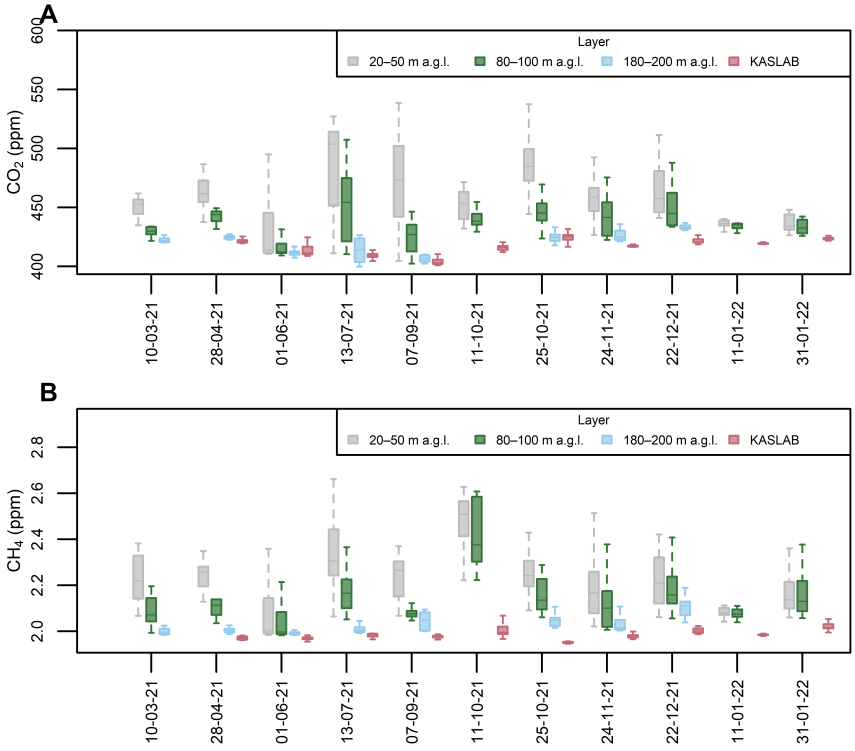

Figure 4. Boxplots of A) CO_2 and B) CH_4 mole fractions measured during flight campaigns at three altitude ranges (20–50 m, 80–100 m, and 180–200 m a.g.l.). The distributions are compared with background concentrations recorded at the KASLAB high-mountain station during the corresponding campaign periods.

of the time of day. The most distinct diurnal variation of the CO_2 profile occurred during the warm season, when biosphere was most active; the highest observed difference between the surface and the free atmosphere of around 150 ~~ppm~~ ppm was observed in autumn. In winter, CO_2 vertical profile varied less, with a minimum observed vertical gradient of 50 ~~ppm~~ppm. In this season, CO_2 net flux from the biosphere, which is a main driver of diurnal variability of surface emissions, is drastically diminished (Zimnoch et al., 2004), so the near-surface CO_2 mole fraction remains influenced mainly by the boundary layer diurnal dynamics. CH_4 diurnal variation ~~was most pronounced in the warm season as well~~has no clear seasonal dependence, with the highest observed mole fraction difference between the surface and free atmosphere of around ~~1.2 ppm occurred during summer night (yellow lines in lower panel of Figure 5). The lowest vertical gradient within the SBL of 0.3 ppm was observed in winter, indicating temperature-dependent methane sources as main drivers of its mole fraction in the surface layer.~~ 0.6 ppm (dark red line on Figure 5A). Similarly to CO_2, BL diurnal dynamics influenced the vertical profiles of methane. It is worth emphasizing that most of the profiles observed between sunset and sunrise show increased concentrations up to a height of 100 ~~m.~~ m a.g.l. which corresponds to the depth of the valley in which Krakow is located. This fact clearly illustrates the influence

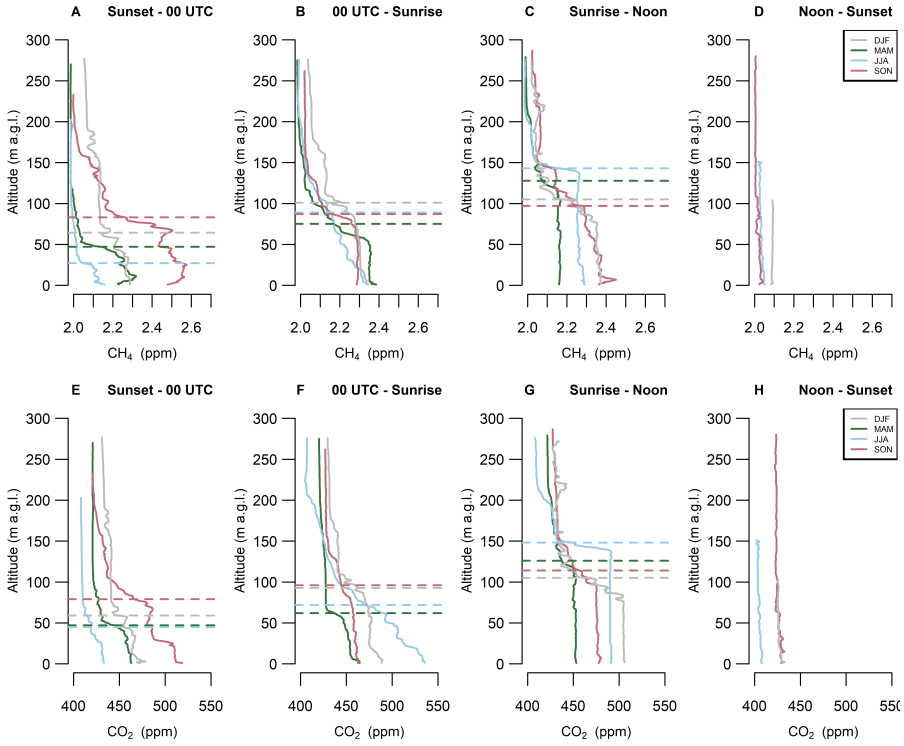

Figure 5. Selected representative CO_2 and CH_4 vertical profiles divided by season (different colours) and time of day (different columns). ~~Solid line repersent balloon profiles while dashed line corresponds~~ The selection was made to ~~the drone profiles. To~~ increase the readability of the graph~~, the number of profiles has been limited~~. The whole dataset is included in the supplement for individual campaigns. Dashed lines on subfigures A-C indicate the boundary layer height determined separately for each individual CO_2 and CH_4 vertical profile.

of local topography on the depth of the ~~inversion layer~~ SBL in the city and the dynamics of vertical mixing of the boundary layer at a stable atmospheric conditions.

A detailed BL dynamics description is included in the following sections. A full overview of the data collected in the scope of this study, grouped by campaign and augmented with meteorological data from the AGH site, is available in the Supplement (Figures S5-S26).

3.2 Atmospheric boundary layer dynamics

3.2.1 Transition from convective boundary layer (CBL) to stable boundary layer (SBL)

Measurements collected during the vertical profiling of UBL confirmed the key influence of UBL dynamics on the vertical profiles of CO_2 and CH_4 ~~molar~~ mole fractions. The evolution of the convective boundary layer and the development of a stable boundary layer is presented in Figure 6 based on results from ~~campaign No. 3. The Campaign was~~ third measurement

campaign (No. 3), carried out from ~~1.06~~01.06.2021 ~~8 UTC until 2.06~~08:00 UTC until 02.06.2021 ~~5 UTC~~(05:00 UTC, with a total of 44 vertical profiles ~~)~~sampled. Because the daytime flights were performed every 10 minutes, to maintain the readability of Figure 6, only the selected profiles representing characteristic situations ~~were presented (11~~ are presented (6 vertical profiles). During the daytime, strong vertical mixing resulted in a constant mole fraction of GHGs in the vertical profile. Between 9 and 16 UTC, the GHG mole fractions in the vertical profile ranged between 408 and 415 ~~ppm~~ ppm for CO_2 and between 1.98 and 2.01 ~~ppm~~ ppm for CH_4, respectively. ~~After~~ Both values were also very close to regional background observed at KASLAB station (Figure 7). A convective character of BL was also confirmed by the temperature profile showing monotonic slightly negative gradient stimulating vertical mixing of BL and almost constant wind speed ranging between 2-4 $m\,s^{-1}$ in a whole profile. After 18 ~~UTC and molar fraction increase was observed close to the ground level. During the night time, a positive temperature gradient (Figure 6-d) and weak wind speed (less than 3~~ UTC, BL dynamics has changed. The wind speed gradually decreased in the lower part of the profile down to ca. 1 $m\,s^{-1}$ ~~- Figure 6-c) up to 100 AGL was observed~~and the temperature gradient has changed to positive value, indicating the formation of an ~~inversion layer.~~ SBL in the first 100-150 m. This situation favored the accumulation of emitted gases near the earth's surface and an increase of CO_2 and CH_4 mole fraction was observed close to the ground level. The vertical CO_2 and CH_4 profiles during this period were characterised by an approximately linear decrease in mole fraction up to an altitude of ca. 100 m ~~AGL.After sumrise~~ a.g.l. After sunrise (last profile) a homogenisation of lower atmospheric part is observed along with inversion of temperature gradient in the first 150 m and a gradual increase in depth and a decrease in the maximum concentration at the ground, which illustrates the initiation of convective movements mixing the ground layer and carrying the gases accumulated at the surface to greater heights. The presence of an inversion aloft above 150 m, observed on temperature profile resulted in a limitation of mixing at higher altitudes and the development of a sharp GHGs gradient at the boundary between the lower convective layer and the inversion aloft. The estimated inverse height marked by a horizontal lines on Figure 6A and B shows gradual increase from creation after sunset by development during the night until decay in the morning. The temporal evolution of CO_2 and CH_4 mole fractions averaged in three altitude ranges (30-50, 80-100, and 150-180 m a.g.l.) along with the regional background level and the marked night period, summarizing the processes discussed is presented on Figure 7.

3.2.2 Transition from stable boundary layer (SBL) to convective boundary layer (CBL)

An example of the evolution from a stable boundary layer through the development of the convective layer occurring in the morning hours is better presented using data from campaign no. 7 (26.10.2021; ~~flights 20-28;~~ Figure 8). The atmospheric temperature, CO_2 and CH_4 vertical profiles show that over ~~4 hours between 5:13~~ five hours between 04:47 UTC and 09:~~22~~ 48 UTC the near-ground temperature inversion (of approximately 7 ~~K~~ °C initially), clearly visible in the ~~first 100 of the atmosphere~~temperature profile, is gradually erased as the increasing surface temperature causes turbulence and mixing, evolving into a well-mixed lower atmosphere when surface temperatures ~~exceed~~ exceeds 10 °C. Initially night-time atmosphere is clearly structured, with ~~high variations~~ enhanced level of CO_2 and CH_4 visible up to 100 m ~~AGL~~ a.g.l. and a distinct elevated CO_2 plumes high aloft (above 200 m ~~AGL~~a.g.l.). These high and vertically localized gradients, together with an elevated and gently varying specific humidity above 100 m ~~AGL~~ a.g.l. point to a strong shear of plumes emitted upwind into a residual

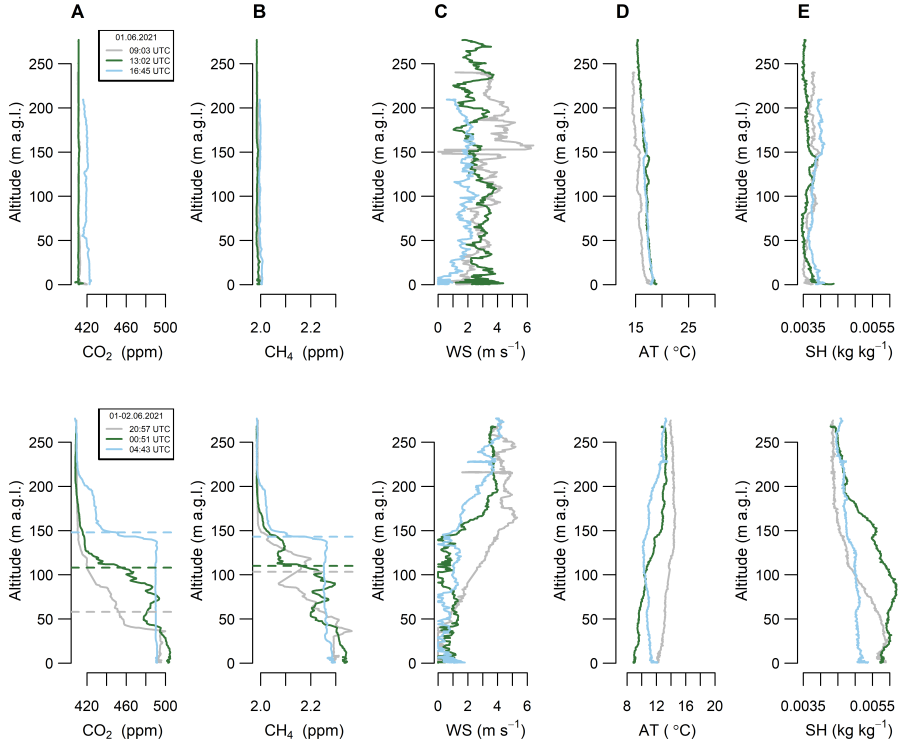

Figure 6. Selected vertical profiles of A) CO_2 and B) CH_4 mole fraction, C) wind speed, D) air temperature and E) specific humidity for campaign No. 3 (01-02.06.2021). Dashed lines on A-B indicate the boundary layer height determined separately for each individual CH_4 and CO_2 vertical profile. Explanations: WS – wind speed, AT – air temperature, SH – specific humidity.

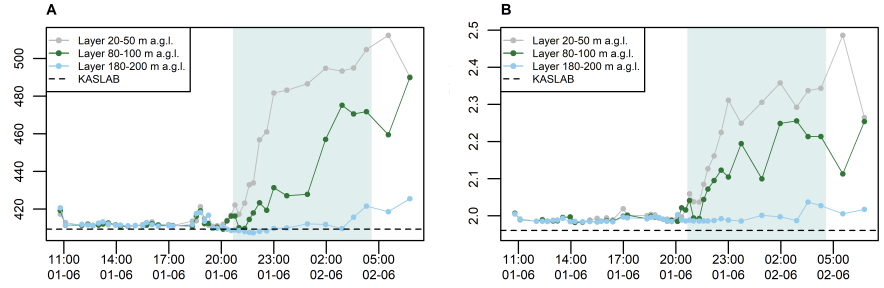

Figure 7. ~~Selected vertical profiles~~ Time course of ~~a~~A) ~~CO_2~~ CO_2 and ~~b~~B) ~~CH_4~~ CH_4 mole ~~fraction, c) wind speed, d) air temperature and e) specific humidity for~~ fractions measured during campaign ~~No~~no. 3 (01-02.06.2021) averaged at three altitude ranges (20–50 m, 80–100 m, and 180–200 m a.g.l.). The averages are compared with regional background recorded at the KASLAB high-mountain station (dashed line) during the corresponding campaign period. Azure background presents night-time period. The regional background was calculated as the 5-th percentile of 10-minute averaged mole fractions from KASLAB station.

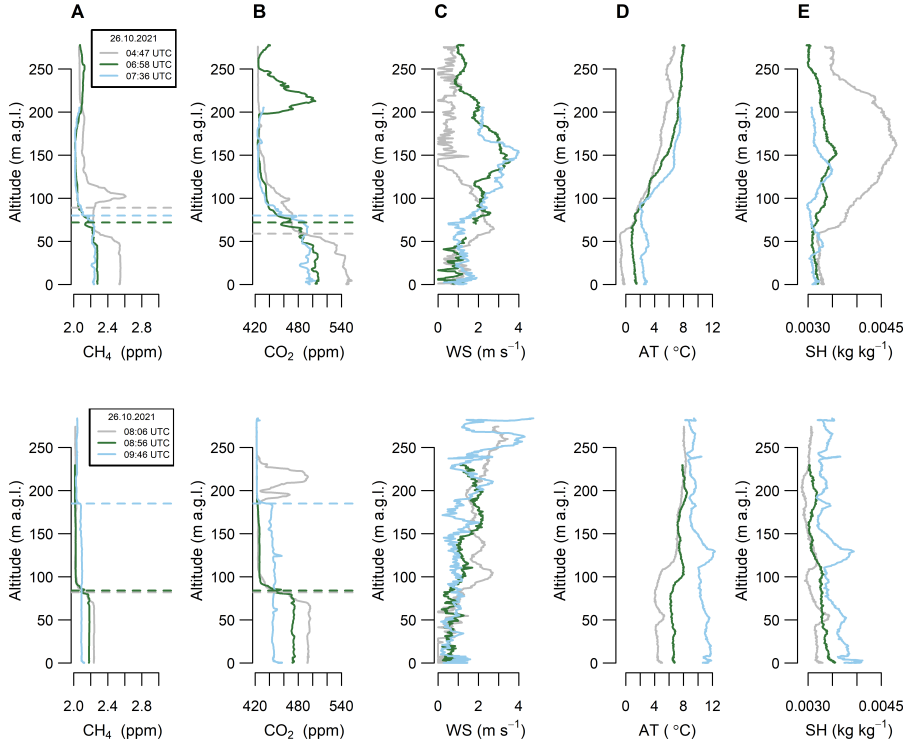

Figure 8. Selected vertical profiles of CH_4 and CO_2 mole ~~fraction~~fractions, wind speed, air temperature, and ~~mole fraction~~ specific humidity measured during sampling campaign no. 7 (26.10.2021). Dashed lines on A-B indicate the boundary layer height determined separately for each individual CH_4 and CO_2 vertical profile. Explanations: WS – wind speed, AT – air temperature, SH – specific humidity.

layer formed on a previous day, transported by varying horizontal winds, strongest at ~~120~~ 150 m ~~AGL at 05:13~~ a.g.l. at 06:58 and 7:36 UTC, and reaching a maximum of 4 $m\,s^{-1}$ ~~at 150 AGL~~. Over the morning, the enhancement in GHG mole fractions develops a well-mixed layer that rises together with the inversion cap, crossing ~~50~~ 90 m ~~AGL between 07:36 UTC and 07:49 UTC~~a.g.l. at 08:56 UTC, and reaching approximately ~~100~~ 180 m ~~AGL~~ a.g.l. at 09:~~22 UTC, after which it continues to rise quickly, and is identifiable at 180 AGL at 09:48 UTC,~~ 46 UTC, which is the last flight of the campaign. A complete set of profiles on that day is available in the Supplement (Figure S17).

Analysis of the time course of mole fractions (Figure 9) averaged for the lower (20-50 m a.g.l.), intermediate (80-100 m a.g.l.), and upper (180-200 m a.g.l.) layers shows a gradual increase in the lower and intermediate layers during the night, followed by a sharp decline shortly after sunrise. The levels observed in the upper layer remain close to the regional background until about 04:00 UTC, after which they begin to gradually increase, indicating the initiation of SBL degradation and the slow transport of accumulated gases to higher regions of the BL. The methane peak observed at 03:00 UTC (Figure 9B) in the intermediate layer may indicate the detection of a plume of this gas originating from a nearby emission source whose height is within SBL. A more detailed analysis of such observed cases can be found in the following subsections.

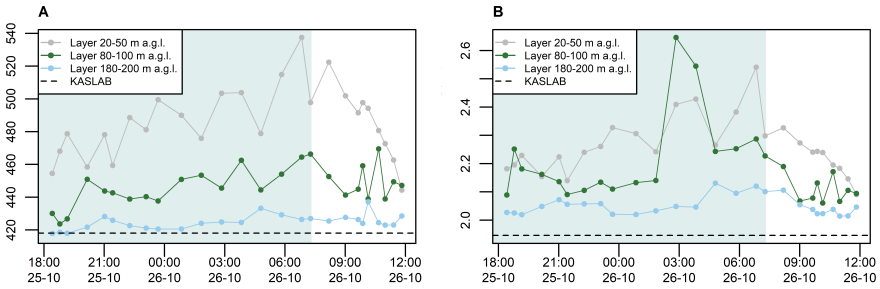

Figure 9. Time course of A) CO_2 and B) CH_4 mole fractions measured during campaign no. 7 (25-26.10.2021) averaged at three altitude ranges (20–50 m, 80–100 m, and 180–200 m a.g.l.). The averages are compared with regional background recorded at the KASLAB high-mountain station (dashed line) during the corresponding campaign period. Azure background presents night-time period. The regional backgreound was calculated as the 5-th percentile of 10-minute averaged mole fractions from KASLAB station.

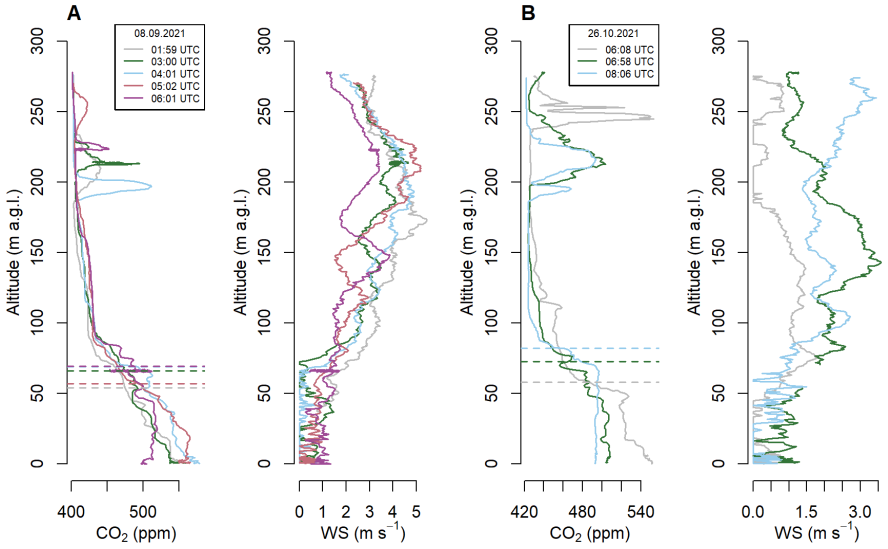

Figure 10. Vertical profiles of CO_2 and wind speed (WS) for specific hours at: ~~a~~A) campaign No. 5 (flights 26–30; date: 08.09.2021) and ~~b~~B) campaign No. 7 (flights 21, 22, 25; date: 26.10.2021). On both nights a plume of CO_2 was observed aloft, between 200–250 m ~~AGL~~a.g.l. Dashed lines indicate the boundary layer height determined separately for each individual CO_2 vertical profile.

3.3 Anomalies in vertical distribution of GHGs - CO_2 case study

Figure 10 presents results from two measurement campaigns for which a plume of CO_2 was visible at an ~~altitude of 200~~ altitudes between 190-230 m ~~AGL~~ a.g.l. (measurements from 8 September 2021) and 200-250 m ~~AGL~~ a.g.l. (measurements from 26 October 2021).

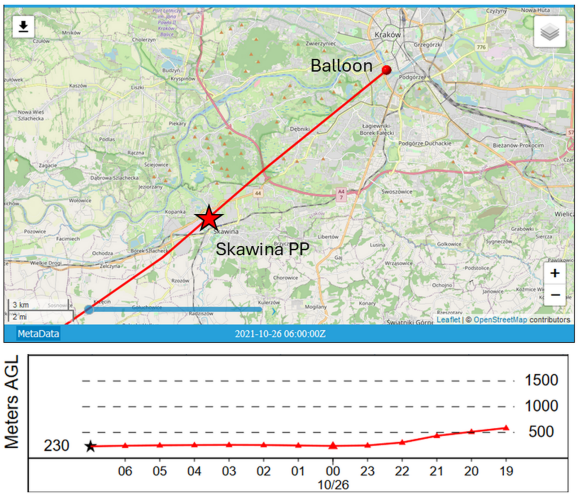

Figure 11. Hysplit back trajectory calculated using GFS0p25 meteo fields for 26.10.2021 6:00 UTC. Starting point in the balloon location at 230 m a.g.l. Position of Skawina PP marked with red star. Lower panel presents trajectory altitude.

Strong maxima of CO_2 mole fractions observed in the vertical profiles measured on 8 September between 01:00 UTC and 06:20 UTC at approximately 200 m ~~AGL~~ a.g.l. are clearly of different origin than gradually increasing signals closer to the surface (Figure 10~~a~~A). Such relatively thin ~~nighttime~~ night-time layers with strong enhancements of CO_2 are often generated by CO_2 tall stack emissions typically associated with power generation or industrial activities located upwind of the measurement point. Due to the weak vertical transport in a stable ~~nighttime~~ night-time atmosphere, such plumes can be transported for long distances.

Based on the prevalent wind conditions on the measurement day, as well as available knowledge on the location of the power plants in the vicinity of Krakow, we hypothesise that the observed signal originates from one of the two nearby co-generation plants~~(Pol. "elektrociepłownia", EC),~~ , each powered by hard coal combustion. Those were ~~EC Skawina and EC Krakow~~ Skawina PP and Kraków PP (Figure 1). As the available measurements of wind speed and direction were sparse and variable in time and the wind patterns are often complex in the urban environment, it was not possible to identify the source responsible for observed CO_2 enhancements based on meteorological ~~parameters only.~~ variables only.

Based on preliminary back-trajectory HySplit model calculations ~~(?), and more detailed analysis of archival data of the operational weather forecast from IMGW-PIB of the AROME model for that day,~~ (Stein et al., 2015; NOAA ARL, 2026), it can be concluded that the observed plume originated from ~~the EC Skawina (not shown in this article~~Skawina PP (Figure 11). Knowing the location of the emission source and terrain properties, presented case may be usefull benchmark for testing of the vertical transport performance in the numerical atmospheric models.

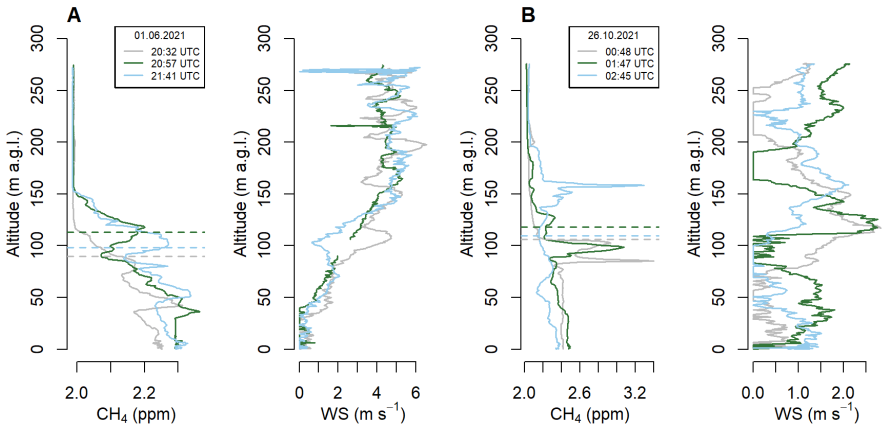

Figure 12. Vertical profiles of CH_4 and wind speed (WS) for specific hours at ~~a~~A) campaign no. 3 (flights 39-41; 01.06.2021) and ~~b~~B) campaign no. 7 (flights 15-17; 26.10.2021), when Gaussian plumes of CH_4 were observed. Dashed lines indicate the boundary layer height determined separately for each individual CH_4 vertical profile.

3.4 Anomalies in greenhouse gas vertical distribution - CH_4 case study

Similar peaks ~~above the inversion layer~~ have been also observed in the case of CH_4 mole fraction (Figure 12), however, the time of detected plumes and their altitude differs from CO_2. In most cases the methane peaks appear within SBL. It suggests that ~~in the case of methane,~~ we were also able to detect the plumes emitted from a point source, but the origin and temporal dynamics of this source are different from CO_2. The lower altitude od detected peaks suggest the location of the emission are not associated with industial sources emmiting methane from stacks at the elevated level (like in case of CO_2). Due to the lack of evident possible source locations, it was not possible to attribute the specific plumes to particular locations. Although the most likely source of emissions are leaks in the city gas network, or sewerage network, identification of emission sources requires further studies using model simulations with more realistic methane emission fields for the city.

4 Conclusions

The measurement report describes 11 ~~monthly-based~~ UBL profiling measurement campaigns conducted between March 2021 and February 2022 in the city of Krakow (Southern Poland) with approximately monthly frequency . The measurements incorporated the basic meteorological ~~parameters~~ variables (temperature, relative humidity, pressure, wind speed) and CO_2 and CH_4 ~~molar~~ mole fractions recorded with 1 s temporal resolution along the profiles ranging from ground level up to 280 m ~~AGL.~~a.g.l. During each campaign, several profiles were collected with at least hourly resolution covering all periods of the day, mainly focused on the formation, development and decaying of the ~~inversion layer~~ SBL within UBL. However, the data also illustrate the influence of terrain on the vertical distribution of trace gas contents in the boundary layer and also contain interesting point source contaminant plume data detected above ~~the inversion layer~~and within the SBL, allowing their use to

test the parameterization of vertical transport under stable atmospheric conditions in numerical atmospheric models.

The case studies presented in this article capture clear temporal and spatial gradients, particularly within the lower PBL. The broader value of this dataset lies in its potential application for model validation. Specifically, the profiles can serve as a benchmark for evaluating regional or mesoscale transport models, offering a means to assess the performance of ~~modeled~~ modelled vertical mixing, advection, and surface flux parametrizations. As such, these data contribute not only to observational insights, but also to the refinement of process-based and inverse modelling approaches within the carbon cycle research community. ~~The identification of signals in UBL indicates the potential for reporting unexpected methane emissions. Identifying the specific sources proved to require more sophisticated data on the spatial emission distribution.~~ From the methodological point of view, we showed that carrying out profile measurements requires instruments capable of fast and precise detection of changes in measured ~~parameters~~ variables (both GHG mole fractions and meteorological variables) which can change rapidly with height. ~~The response time of temperature sensors turned out to be crucial when measuring vertical gradients, indicating the advantage of less inert thermocouple sensors compared to semiconductor sensors.~~ In the case of measuring the wind direction, it turned out that despite corrections using an accelerometer and magnetometer, interference related to the disturbance of the magnetic field by powering the ~~drone~~UAV's engines, or uncontrolled sudden rotational and lateral movements of the tethered balloon during descent caused the measurement ~~being unreliable. Hence, other solutions for this parameter measurement are recommended than the one used here.~~ to be unreliable.

The identification of CH_4 signals in UBL also indicates the potential for reporting unexpected methane emissions. Identifying the specific sources needs to be done in tandem with analysis of spatial emission distribution. This can be achieved by direct analysis of the backward trajectories, like presented here. A more sophisticated approach using a full Bayesian inversion framework is in preparation.

Code and data availability. ERA5 data available via Copernicus Climate Data Store (CDS; Hersbach et al., 2017). The measurements data set is available for download from the ICOS Carbon Portal (https://doi.org/10.18160/8DSK-R4JS; Zimnoch et al., 2023)

Author contributions. MZ, MG, PS conceptualised and prepared the study, and also drafted and finalised the manuscript. MZ, MG, PS, AJK, ŁC processed, analysed and visualised the presented data. All co-authors contributed to the carrying out of the measurement campaigns as well as manuscript preparation.

Competing interests. The authors declare that they have no conflict of interest.

Acknowledgements. The authors would like to thank the crew members of the "Balon Widokowy sp. z o.o." for providing the balloon platform for the experiments and for their support during the campaigns. Without their help, it would not have been possible to conduct the measurements. This project has been partially supported by the European Union's Horizon 2020 research and innovation programme under grant agreements No. 958927 and No. 101037319, and the subsidy of the Ministry of Education and Science. The research results presented in this paper have been developed with the use of equipment financed from the funds of the "Excellence Initiative - Research University" program at AGH University of Krakow. We gratefully acknowledge Polish high-performance computing infrastructure PLGrid (HPC Centers: ACK Cyfronet AGH) for providing computer facilities and support within computational grants no. PLG/2021/014946, PLG/2022/015860, PLG/2023/~~016669 and the "Balon Widokowy sp. z o.o." crew members for providing the balloon platform for the experiments and support during the campaigns~~016669. This research was partially supported by a subsidy from the Polish Ministry of Science and Higher Education.

References

Andersen, T., Scheeren, B., Peters, W., and Chen, H.: A UAV-based active AirCore system for measurements of greenhouse gases, Atmospheric Measurement Techniques, 11, 2683–2699, https://doi.org/10.5194/amt-11-2683-2018, 2018.

Ashworth, K., Bucci, S., Gallimore, P. J., Lee, J., Nelson, B. S., Sanchez-Marroquín, A., Schimpf, M. B., Smith, P. D., Drysdale, W. S., Hopkins, J. R., Lee, J. D., Pitt, J. R., Di Carlo, P., Krejci, R., and McQuaid, J. B.: Megacity and local contributions to regional air pollution: an aircraft case study over London, Atmospheric Chemistry and Physics, 20, 7193–7216, https://doi.org/10.5194/acp-20-7193-2020, 2020.

Bergamaschi, P., Corazza, M., Karstens, U., Athanassiadou, M., Thompson, R. L., Pison, I., Manning, A. J., Bousquet, P., Segers, A., Vermeulen, A. T., Janssens-Maenhout, G., Schmidt, M., Ramonet, M., Meinhardt, F., Aalto, T., Haszpra, L., Moncrieff, J., Popa, M. E., Lowry, D., Steinbacher, M., Jordan, A., O'Doherty, S., Piacentino, S., and Dlugokencky, E.: Top-down estimates of European CH_4 and N_2O emissions based on four different inverse models, Atmospheric Chemistry and Physics, 15, 715–736, https://doi.org/10.5194/acp-15-715-2015, 2015.

Bezyk, Y., Górka, M., Sówka, I., Nęcki, J., and Strąpoć, D.: Temporal dynamics and controlling factors of CO2 and CH4 variability in the urban atmosphere of Wroclaw, Poland, Science of The Total Environment, 893, 164 771, https://doi.org/https://doi.org/10.1016/j.scitotenv.2023.164771, 2023.

Bolek, A., Heimann, M., and Göckede, M.: UAV-based in situ measurements of CO_2 and CH_4 fluxes over complex natural ecosystems, Atmospheric Measurement Techniques, 17, 5619–5636, https://doi.org/10.5194/amt-17-5619-2024, 2024.

Cambaliza, M. O. L., Shepson, P. B., Caulton, D. R., Stirm, B., Samarov, D., Gurney, K. R., Turnbull, J., Davis, K. J., Possolo, A., Karion, A., Sweeney, C., Moser, B., Hendricks, A., Lauvaux, T., Mays, K., Whetstone, J., Huang, J., Razlivanov, I., Miles, N. L., and Richardson, S. J.: Assessment of uncertainties of an aircraft-based mass balance approach for quantifying urban greenhouse gas emissions, Atmospheric Chemistry and Physics, 14, 9029–9050, https://doi.org/10.5194/acp-14-9029-2014, 2014.

Chen, J., Dietrich, F., Forstmaier, A., Bettinelli, J., Maazallahi, H., Schneider, C., Röckmann, T., Winkler, D., Zhao, X., Makowski, M., Klappenbach, F., van der Veen, C., Wildmann, N., Jones, T., Ament, F., Lange, I., Denier van der Gon, H., and Schwietzke, S.: Multi-scale measurements combined with inverse modeling for assessing methane emissions of Hamburg, in: EGU General Assembly 2022, Vienna, Austria, 23–27 May 2022, EGU22-11548, https://doi.org/https://doi.org/10.5194/egusphere-egu22-11548, 2022.

Crawford, B., Christen, A., and McKendry, I.: Diurnal Course of Carbon Dioxide Mixing Ratios in the Urban Boundary Layer in Response to Surface Emissions, Journal of Applied Meteorology and Climatology, 55, 507 – 529, https://doi.org/10.1175/JAMC-D-15-0060.1, 2016.

de Foy, B., Schauer, J. J., Lorente, A., and Borsdorff, T.: Investigating high methane emissions from urban areas detected by TROPOMI and their association with untreated wastewater, Environmental Research Letters, 18, 044 004, https://doi.org/10.1088/1748-9326/acc118, 2023.

Dietrich, F., Chen, J., Voggenreiter, B., Aigner, P., Nachtigall, N., and Reger, B.: MUCCnet: Munich Urban Carbon Column network, Atmospheric Measurement Techniques, 14, 1111–1126, https://doi.org/10.5194/amt-14-1111-2021, 2021.

Duren, R. M. and Miller, C. E.: Measuring the carbon emissions of megacities, Nature Climate Change, 2, 560–562, https://doi.org/10.1038/nclimate1629, 2012.

ECMWF: COCO2 Project Website, website, last access: 15 Feb 2026, https://coco2-project.eu/, 2026.

EEA: Industrial Reporting under the Industrial Emissions Directive 2010/75/EU and European Pollutant Release and Transfer Register Regulation (EC) No 166/2006 - ver. 10.0 Dec 2023 (Tabular data), https://doi.org/10.2909/63a14e09-d1f5-490d-80cf-6921e4e69551, 2023.

Enting, I. G., Trudinger, C. M., and Francey, R. J.: A synthesis inversion of the concentration and δ13 C of atmospheric CO2, Tellus B, 47, 35–52, https://doi.org/https://doi.org/10.1034/j.1600-0889.47.issue1.5.x, 1995.

Fiehn, A., Kostinek, J., Eckl, M., Klausner, T., Gałkowski, M., Chen, J., Gerbig, C., Röckmann, T., Maazallahi, H., Schmidt, M., Korbeń, P., Nęçki, J., Jagoda, P., Wildmann, N., Mallaun, C., Bun, R., Nickl, A.-L., Jöckel, P., Fix, A., and Roiger, A.: Estimating CH_4, CO_2 and CO emissions from coal mining and industrial activities in the Upper Silesian Coal Basin using an aircraft-based mass balance approach, Atmospheric Chemistry and Physics, 20, 12 675–12 695, https://doi.org/10.5194/acp-20-12675-2020, 2020.

Gałkowski, M., Jordan, A., Rothe, M., Marshall, J., Koch, F.-T., Chen, J., Agusti-Panareda, A., Fix, A., and Gerbig, C.: In situ observations of greenhouse gases over Europe during the CoMet 1.0 campaign aboard the HALO aircraft, Atmospheric Measurement Techniques, 14, 1525–1544, https://doi.org/10.5194/amt-14-1525-2021, 2021.

Gerbig, C., Lin, J. C., Wofsy, S. C., Daube, B. C., Andrews, A. E., Stephens, B. B., Bakwin, P. S., and Grainger, C. A.: Toward constraining regional-scale fluxes of CO2 with atmospheric observations over a continent: 1. Observed spatial variability from airborne platforms, Journal of Geophysical Research: Atmospheres, 108, https://doi.org/https://doi.org/10.1029/2002JD003018, 2003.

Giovannini, L., Ferrero, E., Karl, T., Rotach, M. W., Staquet, C., Trini Castelli, S., and Zardi, D.: Atmospheric Pollutant Dispersion over Complex Terrain: Challenges and Needs for Improving Air Quality Measurements and Modeling, Atmosphere, 11, https://doi.org/10.3390/atmos11060646, 2020.

Hedworth, H., Page, J., Sohl, J., and Saad, T.: Investigating Errors Observed during UAV-Based Vertical Measurements Using Computational Fluid Dynamics, Drones, 6, https://doi.org/10.3390/drones6090253, 2022.

Heimburger, A. M. F., Harvey, R. M., Shepson, P. B., Stirm, B. H., Gore, C., Turnbull, J., Cambaliza, M. O. L., Salmon, O. E., Kerlo, A.-E. M., Lavoie, T. N., Davis, K. J., Lauvaux, T., Karion, A., Sweeney, C., Brewer, W. A., Hardesty, R. M., and Gurney, K. R.: Assessing the optimized precision of the aircraft mass balance method for measurement of urban greenhouse gas emission rates through averaging, Elementa: Science of the Anthropocene, 5, 26, https://doi.org/10.1525/elementa.134, 2017.

Hersbach, H., Bell, B., Berrisford, P., Hirahara, S., Horányi, A., Muñoz-Sabater, J., Nicolas, J., Peubey, C., Radu, R., Schepers, D., Simmons, A., Soci, C., Abdalla, S., Abellan, X., Balsamo, G., Bechtold, P., Biavati, G., Bidlot, J., Bonavita, M., De Chiara, G., Dahlgren, P., Dee, D., Diamantakis, M., Dragani, R., Flemming, J., Forbes, R., Fuentes, M., Geer, A., Haimberger, L., Healy, S., Hogan, R. J., Hólm, E., Janisková, M., Keeley, S., Laloyaux, P., Lopez, P., Lupu, C., Radnoti, G., de Rosnay, P., Rozum, I., Vamborg, F., Villaume, S., and Thépaut, J.-N.: Complete ERA5 global atmospheric reanalysis, Dataset, https://doi.org/10.24381/cds.143582cf, 2017.

Hoheisel, A., Couret, C., Hellack, B., and Schmidt, M.: Comparison of atmospheric CO, CO_2 and CH_4 measurements at the Schneefernerhaus and the mountain ridge at Zugspitze, Atmospheric Measurement Techniques, 16, 2399–2413, https://doi.org/10.5194/amt-16-2399-2023, 2023.

Honnert, R., Efstathiou, G. A., Beare, R. J., Ito, J., Lock, A., Neggers, R., Plant, R. S., Shin, H. H., Tomassini, L., and Zhou, B.: The Atmospheric Boundary Layer and the "Gray Zone" of Turbulence: A Critical Review, Journal of Geophysical Research: Atmospheres, 125, e2019JD030 317, https://doi.org/https://doi.org/10.1029/2019JD030317, e2019JD030317 10.1029/2019JD030317, 2020.

ICOS-Cities: ICOS-Cities, website, last access: February 14th, 2026, https://www.icos-cp.eu/projects/icos-cities, 2026.

ICOS RI: ICOS Atmosphere Station Specifications V2.0 (editor: O. Laurent), Tech. rep., ICOS Research Infrastructure, https://doi.org/10.18160/GK28-2188, 2020.

IEA: World Energy Outlook, chap. 8, pp. 179–193, International Energy Agency, 2008.

IMGW-PIB: IMGW-PIB forecasts, website, last access: June 2nd, 2023, meteo.imgw.pl, 2023.

IPCC: Climate Change 2023: Synthesis Report. Contribution of Working Groups I, II and III to the Sixth Assessment Report of the Intergovernmental Panel on Climate Change, pp. 35–115, IPCC, Geneva, Switzerland, https://doi.org/10.59327/IPCC/AR6-9789291691647, 2023.

Jasek-Kamińska, A., Zimnoch, M., Wachniew, P., and Różański, K.: Urban CO2 Budget: Spatial and Seasonal Variability of CO2 Emissions in Krakow, Poland, Atmosphere, 11, https://doi.org/10.3390/atmos11060629, 2020.

Keppel-Aleks, G., Wennberg, P. O., and Schneider, T.: Sources of variations in total column carbon dioxide, Atmospheric Chemistry and Physics, 11, 3581–3593, https://doi.org/10.5194/acp-11-3581-2011, 2011.

Klausner, T., Mertens, M., Huntrieser, H., Galkowski, M., Kuhlmann, G., Baumann, R., Fiehn, A., Jöckel, P., Pühl, M., and Roiger, A.: Urban greenhouse gas emissions from the Berlin area: A case study using airborne CO2 and CH4 in situ observations in summer 2018, Elementa: Science of the Anthropocene, 8, https://doi.org/10.1525/elementa.411, 15, 2020.

Kotthaus, S., Haeffelin, M., Drouin, M.-A., Dupont, J.-C., Grimmond, S., Haefele, A., Hervo, M., Poltera, Y., and Wiegner, M.: Tailored Algorithms for the Detection of the Atmospheric Boundary Layer Height from Common Automatic Lidars and Ceilometers (ALC), Remote Sensing, 12, https://doi.org/10.3390/rs12193259, 2020.

Krings, T., Neininger, B., Gerilowski, K., Krautwurst, S., Buchwitz, M., Burrows, J. P., Lindemann, C., Ruhtz, T., Schüttemeyer, D., and Bovensmann, H.: Airborne remote sensing and in situ measurements of atmospheric CO_2 to quantify point source emissions, Atmospheric Measurement Techniques, 11, 721–739, https://doi.org/10.5194/amt-11-721-2018, 2018.

Kunz, M., Lavric, J. V., Gerbig, C., Tans, P., Neff, D., Hummelgård, C., Martin, H., Rödjegård, H., Wrenger, B., and Heimann, M.: COCAP: a carbon dioxide analyser for small unmanned aircraft systems, Atmospheric Measurement Techniques, 11, 1833–1849, https://doi.org/10.5194/amt-11-1833-2018, 2018.

Lampert, A., Pätzold, F., Asmussen, M. O., Lobitz, L., Krüger, T., Rausch, T., Sachs, T., Wille, C., Sotomayor Zakharov, D., Gaus, D., Bansmer, S., and Damm, E.: Studying boundary layer methane isotopy and vertical mixing processes at a rewetted peatland site using an unmanned aircraft system, Atmospheric Measurement Techniques, 13, 1937–1952, https://doi.org/10.5194/amt-13-1937-2020, 2020.

Lauvaux, T., Miles, N. L., Richardson, S. J., Deng, A., Stauffer, D. R., Davis, K. J., Jacobson, G., Rella, C., Calonder, G.-P., and DeCola, P. L.: Urban Emissions of CO2 from Davos, Switzerland: The First Real-Time Monitoring System Using an Atmospheric Inversion Technique, Journal of Applied Meteorology and Climatology, 52, 2654 – 2668, https://doi.org/10.1175/JAMC-D-13-038.1, 2013.

Lauvaux, T., Miles, N. L., Deng, A., Richardson, S. J., Cambaliza, M. O., Davis, K. J., Gaudet, B., Gurney, K. R., Huang, J., O'Keefe, D., Song, Y., Karion, A., Oda, T., Patarasuk, R., Razlivanov, I., Sarmiento, D., Shepson, P., Sweeney, C., Turnbull, J., and Wu, K.: High-resolution atmospheric inversion of urban CO2 emissions during the dormant season of the Indianapolis Flux Experiment (INFLUX), Journal of Geophysical Research: Atmospheres, 121, 5213–5236, https://doi.org/10.1002/2015JD024473, 2016.

Li, Y., Deng, J., Mu, C., Xing, Z., and Du, K.: Vertical distribution of CO2 in the atmospheric boundary layer: Characteristics and impact of meteorological variables, Atmospheric Environment, 91, 110–117, https://doi.org/https://doi.org/10.1016/j.atmosenv.2014.03.067, 2014.

Lopez-Coto, I., Hicks, M., Karion, A., Sakai, R. K., Demoz, B., Prasad, K., and Whetstone, J.: Assessment of Planetary Boundary Layer Parameterizations and Urban Heat Island Comparison: Impacts and Implications for Tracer Transport, Journal of Applied Meteorology and Climatology, 59, 1637 – 1653, https://doi.org/10.1175/JAMC-D-19-0168.1, 2020a.

Lopez-Coto, I., Ren, X., Salmon, O. E., Karion, A., Shepson, P. B., Dickerson, R. R., Stein, A., Prasad, K., and Whetstone, J. R.: Wintertime CO2, CH4, and CO Emissions Estimation for the Washington, DC–Baltimore Metropolitan Area Using an Inverse Modeling Technique, Environmental Science & Technology, 54, 2606–2614, https://doi.org/10.1021/acs.est.9b06619, 2020b.

Lowry, D., Holmes, C. W., Rata, N. D., O'Brien, P., and Nisbet, E. G.: London methane emissions: Use of diurnal changes in concentration and δ13C to identify urban sources and verify inventories, Journal of Geophysical Research: Atmospheres, 106, 7427–7448, https://doi.org/https://doi.org/10.1029/2000JD900601, 2001.

Mays, K. L., Shepson, P. B., Stirm, B. H., Karion, A., Sweeney, C., and Gurney, K. R.: Aircraft-Based Measurements of the Carbon Footprint of Indianapolis, Environmental Science & Technology, 43, 7816–7823, https://doi.org/10.1021/es901326b, 2009.

McKinney, K. A., Wang, D., Ye, J., de Fouchier, J.-B., Guimarães, P. C., Batista, C. E., Souza, R. A. F., Alves, E. G., Gu, D., Guenther, A. B., and Martin, S. T.: A sampler for atmospheric volatile organic compounds by copter unmanned aerial vehicles, Atmospheric Measurement Techniques, 12, 3123–3135, https://doi.org/10.5194/amt-12-3123-2019, 2019.

Menoud, M., van der Veen, C., Necki, J., Bartyzel, J., Szénási, B., Stanisavljević, M., Pison, I., Bousquet, P., and Röckmann, T.: Methane (CH_4) sources in Krakow, Poland: insights from isotope analysis, Atmospheric Chemistry and Physics, 21, 13 167–13 185, https://doi.org/10.5194/acp-21-13167-2021, 2021.

Nalini, K., Lauvaux, T., Abdallah, C., Lian, J., Ciais, P., Utard, H., Laurent, O., and Ramonet, M.: High-Resolution Lagrangian Inverse Modeling of CO2 Emissions Over the Paris Region During the First 2020 Lockdown Period, Journal of Geophysical Research: Atmospheres, 127, e2021JD036 032, https://doi.org/https://doi.org/10.1029/2021JD036032, e2021JD036032 2021JD036032, 2022.

Nautical Almanac Office: Almanac for computers, United States Naval Observatory, Washington, DC, 1990.

NIES: GOSAT-2, website, last access: June 2nd, 2023, www.gosat-2.nies.go.jp, 2023.

NOAA: Trends in Atmospheric Carbon Dioxide, web press release, last access: 15 May 2024, https://www.noaa.gov/news-release/greenhouse-gases-continued-to-increase-rapidly-in-2022, 2024.

NOAA ARL: Hysplit-web (internet-based) by NOAA Air Resources Laboratory, website, last access 16.02.2026, https://www.ready.noaa.gov/HYSPLIT.php, 2026.

Ou, Y., Roney, C., Alsalam, J., Calvin, K., Creason, J., Edmonds, J., Fawcett, A. A., Kyle, P., Narayan, K., O'Rourke, P., Patel, P., Ragnauth, S., Smith, S. J., and McJeon, H.: Deep mitigation of CO2 and non-CO2 greenhouse gases toward 1.5 °C and 2 °C futures, Nature Communications, 12, 6245, https://doi.org/10.1038/s41467-021-26509-z, 2021.

Park, H., Jeong, S., Sha, M. K., Lee, J., and Frey, M. M.: Comparisons of Greenhouse Gas Observation Satellite Performances Over Seoul Using a Portable Ground-Based Spectrometer, Geophysical Research Letters, 51, e2024GL109 334, https://doi.org/https://doi.org/10.1029/2024GL109334, e2024GL109334 2024GL109334, 2024.

Park, M.-S., Park, S.-H., Chae, J.-H., Choi, M.-H., Song, Y., Kang, M., and Roh, J.-W.: High-resolution urban observation network for user-specific meteorological information service in the Seoul Metropolitan Area, South Korea, Atmospheric Measurement Techniques, 10, 1575–1594, https://doi.org/10.5194/amt-10-1575-2017, 2017.

Peng, Y., Hu, C., Ai, X., Li, Y., Gao, L., Liu, H., Zhang, J., and Xiao, W.: Improvements of Simulating Urban Atmospheric CO2 Concentration by Coupling with Emission Height and Dynamic Boundary Layer Variations in WRF-STILT Model, Atmosphere, 14, https://doi.org/10.3390/atmos14020223, 2023.

Ponomarev, N., Steiner, M., Koene, E., Rubli, P., Grange, S., Constantin, L., Ramonet, M., David, L., Hamzehloo, A., Emmenegger, L., and Brunner, D.: Estimation of CO_2 fluxes in the cities of Zurich and Paris using the ICON-ART CTDAS inverse modelling framework, Atmospheric Chemistry and Physics, 26, 547–570, https://doi.org/10.5194/acp-26-547-2026, 2026.

Programme, U. N. E.: Emissions Gap Report 2025: Off Target - Continued Collective inaction puts Global Temperature Goal at Risk, https://doi.org/https://doi.org/10.59117/20.500.11822/48854, 2025.

Reum, F., Gerbig, C., Lavric, J. V., Rella, C. W., and Göckede, M.: Correcting atmospheric CO_2 and CH_4 mole fractions obtained with Picarro analyzers for sensitivity of cavity pressure to water vapor, Atmospheric Measurement Techniques, 12, 1013–1027, https://doi.org/10.5194/amt-12-1013-2019, 2019.

Richardson, S. J., Miles, N. L., Davis, K. J., Lauvaux, T., Martins, D. K., Turnbull, J. C., McKain, K., Sweeney, C., and Cambaliza, M. O. L.: Tower measurement network of in-situ CO2, CH4, and CO in support of the Indianapolis FLUX (INFLUX) Experiment, Elementa: Science of the Anthropocene, 5, https://doi.org/10.1525/elementa.140, 59, 2017.

Rödenbeck, C., Houweling, S., Gloor, M., and Heimann, M.: CO_2 flux history 1982–2001 inferred from atmospheric data using a global inversion of atmospheric transport, Atmospheric Chemistry and Physics, 3, 1919–1964, https://doi.org/10.5194/acp-3-1919-2003, 2003.

Rózanski, K., Chmura, L., Galkowski, M., Necki, J., Zimnoch, M., Bartyzel, J., and O'Doherty, S.: Monitoring of Greenhouse Gases in the Atmosphere - A Polish Perspective, International Geosphere Biospehere Programme: A Study of Global Change.Papers on Global Change IGBP, 23, 111–126, https://www.proquest.com/scholarly-journals/monitoring-greenhouse-gases-atmosphere-polish/docview/1876533397/se-2, copyright - Copyright De Gruyter Open Sp. z o.o. 2016; Last updated - 2024-10-07; SubjectsTermNotLitGenreText - Environmental, 2016.

Sekuła, P., Bokwa, A., Bartyzel, J., Bochenek, B., Chmura, Ł., Gałkowski, M., and Zimnoch, M.: Measurement report: Effect of wind shear on PM_{10} concentration vertical structure in the urban boundary layer in a complex terrain, Atmospheric Chemistry and Physics, 21, 12 113–12 139, https://doi.org/10.5194/acp-21-12113-2021, 2021a.

Sekuła, P., Bokwa, A., Ustrnul, Z., Zimnoch, M., and Bochenek, B.: The impact of a foehn wind on PM10 concentrations and the urban boundary layer in complex terrain: a case study from Kraków, Poland, Tellus B: Chemical and Physical Meteorology, https://doi.org/10.1080/16000889.2021.1933780, 2021b.

Sekuła, P., Zimnoch, M., Bartyzel, J., Bokwa, A., Kud, M., and Necki, J.: Ultra-Light Airborne Measurement System for Investigation of Urban Boundary Layer Dynamics., Sensors (Basel), 21, https://doi.org/10.3390/s21092920, 2021c.

Seto, K., Dhakal, S., Bigio, A., Blanco, H., Delgado, G. C., Dewar, D., Huang, L., Inaba, A., Kansal, A., Lwasa, S., McMahon, J., Müller, D. B., Murakami, J., Nagendra, H., and Ramaswami, A.: Human settlements, infrastructure and spatial planning, chap. 12, Cambridge University Press, Cambridge, UK and New York, NY, USA, 2014.

Stein, A. F., Draxler, R. R., Rolph, G. D., Stunder, B. J. B., Cohen, M. D., and Ngan, F.: NOAA's HYSPLIT Atmospheric Transport and Dispersion Modeling System, Bulletin of the American Meteorological Society, 96, 2059–2077, https://doi.org/10.1175/BAMS-D-14-00110.1, 2015.

TCCON: TCCON, website, last access: June 2nd, 2023, http://www.tccon.caltech.edu/, 2023.

Turnbull, J. C., Karion, A., Fischer, M. L., Faloona, I., Guilderson, T., Lehman, S. J., Miller, B. R., Miller, J. B., Montzka, S., Sherwood, T., Saripalli, S., Sweeney, C., and Tans, P. P.: Assessment of fossil fuel carbon dioxide and other anthropogenic trace gas emissions from airborne measurements over Sacramento, California in spring 2009, Atmospheric Chemistry and Physics, 11, 705–721, https://doi.org/10.5194/acp-11-705-2011, 2011.

UN: Paris Agreement to the United Nations Framework Convention on Climate Change, Dec. 12, 2015, TIAS No. 16–1104, 2015.

USK: Urząd Statystyczny w Krakowie, website, last access: June 2nd, 2023, https://krakow.stat.gov.pl/, 2023.

van der Woude, A. M., de Kok, R., Smith, N., Luijkx, I. T., Botía, S., Karstens, U., Kooijmans, L. M. J., Koren, G., Meijer, H. A. J., Steeneveld, G.-J., Storm, I., Super, I., Scheeren, H. A., Vermeulen, A., and Peters, W.: Near-real-time CO_2 fluxes from CarbonTracker

Europe for high-resolution atmospheric modeling, Earth System Science Data, 15, 579–605, https://doi.org/10.5194/essd-15-579-2023, 2023.

Veefkind, J., Aben, I., McMullan, K., Förster, H., de Vries, J., Otter, G., Claas, J., Eskes, H., de Haan, J., Kleipool, Q., van Weele, M., Hasekamp, O., Hoogeveen, R., Landgraf, J., Snel, R., Tol, P., Ingmann, P., Voors, R., Kruizinga, B., Vink, R., Visser, H., and Levelt, P.: TROPOMI on the ESA Sentinel-5 Precursor: A GMES mission for global observations of the atmospheric composition for climate, air quality and ozone layer applications, Remote Sensing of Environment, 120, 70–83, https://doi.org/https://doi.org/10.1016/j.rse.2011.09.027, the Sentinel Missions - New Opportunities for Science, 2012.

Wei, C., Wang, M., Fu, Q., Dai, C., Huang, R., and Bao, Q.: Temporal characteristics of greenhouse gases (CO2 and CH4) in the megacity Shanghai, China: Association with air pollutants and meteorological conditions, Atmospheric Research, 235, 104 759, https://doi.org/https://doi.org/10.1016/j.atmosres.2019.104759, 2020.

WMO: Integrated Global Greenhouse Gas Information System: Urban Emission Observation and Monitoring Good Research Practice Guidelines, GAW Report No. 314, https://doi.org/https://doi.org/10.59327/WMO/GAW/314, 2025.

Wolff, S., Ehret, G., Kiemle, C., Amediek, A., Quatrevalet, M., Wirth, M., and Fix, A.: Determination of the emission rates of CO_2 point sources with airborne lidar, Atmospheric Measurement Techniques, 14, 2717–2736, https://doi.org/10.5194/amt-14-2717-2021, 2021.

Xueref-Remy, I., Dieudonné, E., Vuillemin, C., Lopez, M., Lac, C., Schmidt, M., Delmotte, M., Chevallier, F., Ravetta, F., Perrussel, O., Ciais, P., Bréon, F.-M., Broquet, G., Ramonet, M., Spain, T. G., and Ampe, C.: Diurnal, synoptic and seasonal variability of atmospheric CO_2 in the Paris megacity area, Atmospheric Chemistry and Physics, 18, 3335–3362, https://doi.org/10.5194/acp-18-3335-2018, 2018.

Zhang, L., Davis, K. J., Schuh, A. E., Jacobson, A. R., Pal, S., Cui, Y. Y., Baker, D., Crowell, S., Chevallier, F., Remaud, M., Liu, J., Weir, B., Philip, S., Johnson, M. S., Deng, F., and Basu, S.: Multi-Season Evaluation of CO2 Weather in OCO-2 MIP Models, Journal of Geophysical Research: Atmospheres, 127, e2021JD035 457, https://doi.org/https://doi.org/10.1029/2021JD035457, e2021JD035457 2021JD035457, 2022.

Zhou, Y., Qiao, C., Zhou, M., Wang, Y., Tian, X., Wang, Y., and Duan, M.: Observation of greenhouse gas vertical profiles in the boundary layer of the Mount Qomolangma region using a multirotor UAV, Atmospheric Measurement Techniques, 18, 1609–1619, https://doi.org/10.5194/amt-18-1609-2025, 2025.

Zimnoch, M., Florkowski, T., Necki, J. M., and Neubert, R. E. M.: Diurnal variability of δ13C and δ18O of atmospheric CO2 in the urban atmosphere of Kraków, Poland, Isotopes in Environmental and Health Studies, 40, 129–143, https://doi.org/10.1080/10256010410001670989, pMID: 15223666, 2004.

Zimnoch, M., Necki, J., Chmura, L., Jasek, A., Jelen, D., Galkowski, M., Kuc, T., Gorczyca, Z., Bartyzel, J., and Rozanski, K.: Quantification of carbon dioxide and methane emissions in urban areas: source apportionment based on atmospheric observations, Mitigation and Adaptation Strategies for Global Change, 24, 1051–1071, https://doi.org/10.1007/s11027-018-9821-0, 2019.

Zimnoch, M., Sekula, P., Jasek-Kaminska, A., Skiba, A., Gałkowski, M., Chmura, L., Bartyzel, J., Jagoda, P., Kud, M., and Necki, J.: Observational datasets of urban CO2 fluxes, atmospheric vertical profiles of CO2 and CH4 and 14CO2, and isotopic composition of atmospheric CO2 at Krakow, Poland; period 2021-2023; part of the CoCO2 project, Dataset, https://doi.org/10.18160/8DSK-R4JS, 2023.